JSTER | JOURNAL OF SCIENTIFIC, TECHNOLOGY AND ENGINEERING RESEARCH

Bilim, Teknoloji ve Mühendislik Araştırmaları Dergisi
***ISSN*: 2717-8404**
Cilt/*Volume*: 6 Sayı/Issue: 1-2 Yıl/*Year*: 2025

JOURNAL

SCIENTIFIC | TECHNOLOGY | ENGINEERING

Bilim ⊕ Teknoloji ⊕ Mühendislik

JSTER

JOURNAL OF SCIENTIFIC, TECHNOLOGY AND ENGINEERING RESEARCH

Bilim, Teknoloji ve Mühendislik Araştırmaları Dergisi

Cilt/*Volume*: 6 Sayı/*Number*: 1 Yıl/*Year*: 2025

***ISSN*: 2717-8404**

CONTENTS / İÇİNDEKİLER

Research Article / Araştırma Makalesi

JOURNAL OF SCIENCE, TECHNOLOGY AND ENGINEERING RESEARCH
Bilim, Teknoloji ve Mühendislik Araştırmaları Dergisi
ISSN (Online) 2717-8404
Available *online* at https://dergipark.org.tr/en/pub/jster

RESEARCH ARTICLE

The Effect of Managerial Support on Employee Creativity: A Study on Aircraft Maintenance Personnel

[*] Neşet Vefa Erden,

[*]Istanbul Nisantasi University, Faculty of Engineering, Industrial Engineering Department, Istanbul, Turkiye
nesetvefa.erden@nisantasi.edu.tr,https://orcid.org/0009-0008-2654-6067

Citation:
Author, A., Author, B. (2025). *The Effect of Managerial Support on Employee Creativity: A Study on Aircraft Maintenance Personnel*, Journal of Science Technology and Engineering Research, 6(1): 1-10. DOI: 10.53525/jster.1620551

HIGHLIGHTS

- *This is the first study to examine the effect of manager support on employee creativity in aircraft maintenance organizations.*
- *A positive and strong relationship was found between manager support and employee creativity.*
- *Both manager support and employee creativity variables do not differ significantly according to demographic characteristics.*
- *The results of the study have important implications for the development of managerial mechanisms to support creative thinking in the aviation industry.*

Article Info

Received: January 15, 2025
Accepted: January 17, 2025

DOI:
10.53525/jster.1620551

***Corresponding Author:**
Neşet Vefa Erden
nesetvefa.erden@nisantasi.edu.tr
Phone: +90 530 553 0310

ABSTRACT

This study aims to examine the effect of managerial support on employee creativity in SHY-145 approved aircraft maintenance organizations operating in Turkey and authorized by the Directorate General of Civil Aviation (DGCA). A quantitative research method was adopted in the study and a relational survey model was used. Data were collected from 362 technical personnel selected by convenience sampling method. A questionnaire form consisting of three sections was used as a data collection tool, and in addition to demographic information, Manager Support Scale and Employee Creativity Scale were applied. According to the regression analysis results, managerial support has a positive and significant effect on employee creativity. Analyses conducted according to demographic variables revealed that both managerial support and employee creativity variables did not show a significant difference according to gender, marital status, age and professional experience groups. In line with the results of the study, it is recommended that creative leadership training programs should be organized for managers in aircraft maintenance organizations, formal mechanisms should be established where technical personnel can share their creative ideas, performance evaluation systems should be restructured to encourage creative thinking, and regulations should be included in DGCA regulations to encourage creative thinking. In future studies, it is suggested investigating the moderating effects of variables such as organizational culture, technological competence and job security climate and conducting comparative studies covering aircraft maintenance organizations in different countries.

Keywords:*Managerial Support, Employee Creativity, Aircraft Maintenance Personnel*.

I. INTRODUCTION

The aviation industry is one that requires high reliability and has a minimum level of fault tolerance. Aircraft maintenance activities in the aviation industry are of vital importance for the safe and efficient maintenance of flight operations [1]. The success of maintenance activities largely depends on the performance of technical personnel working in this field. Aircraft maintenance technicians need to be able to use creative thinking and problem solving skills to produce fast and effective solutions to the technical problems they encounter [2].

The fact that approximately 12-20% of aircraft accidents are caused by maintenance errors [3] reveals the importance of the performance and creativity of aircraft maintenance personnel. Improving the creative thinking and problem solving skills of aircraft maintenance technicians is important for both increasing flight safety and optimizing maintenance costs [4]. A supportive management approach is needed for maintenance personnel to reveal their creative potential. Managerial support emerges as an important factor that helps employees to do their jobs more effectively, reduces stress in the workplace and increases employee creativity [5].

In the literature, three main dimensions of managerial support are proposed as emotional, material and informational support [6]. The presence of managerial support enables employees to unleash their creative potential and produce innovative solutions to the technical problems they face. Understanding the impact of managerial support on employee creativity is of great importance, especially in high-reliability sectors such as aviation.

A review of the literature reveals that there are no studies examining the relationship between managerial support and employee creativity in aircraft maintenance organizations. Existing studies in the aviation sector generally focus on technical issues and there are limited number of studies on organizational behaviour. In this context, the lack of research on the effect of managerial support on employee creativity in aircraft maintenance organizations emerges as an important research problem.

The main purpose of the study is to examine the effect of managerial support on employee creativity in the aircraft maintenance sector. The study was conducted on technical personnel working in SHY-145 approved aircraft maintenance organizations operating in Turkey and authorized by the Directorate General of Civil Aviation (DGCA). The results of the study are expected to fill an important gap in the literature by examining the relationship between managerial support and employee creativity, especially in aircraft maintenance organizations in Turkey. In addition, the results of the study are expected to contribute to the development of human resource management practices in aircraft maintenance organizations and to increase the effectiveness of maintenance activities.

II. METHOD

This study was designed with the relational survey model, one of the quantitative research approaches [7, 8]. The independent variable of the study is managerial support and the dependent variable is employee creativity. In the study, the hypotheses "*H1: Managerial support perceived by aircraft maintenance personnel positively affects employee creativity"* and *" H2: Managerial support perceived by aircraft maintenance personnel and employee creativity differ significantly according to demographic characteristics"* were tested.

The population of the study consists of 4,684 technical personnel working in SHY-145 approved aircraft maintenance organizations operating in Turkey [9]. The minimum sample size was determined as 356 people, and 362 people were contacted in the study [8]. Simple random sampling method was used in sample selection [7], and the criteria were that the participants should have at least one year of current maintenance organization experience, work directly under a manager and take part in active aircraft maintenance activities.

A questionnaire technique was used as a data collection tool. In order to measure managerial support, the unidimensional "Managerial Support Scale" consisting of 7 items was used [10, 11]. The reported Cronbach's alpha reliability coefficient of the scale is 0.918. In order to measure employee creativity, the unidimensional "Employee

Creativity Scale" consisting of 11 items was used[12]. The reported Cronbach's alpha reliability coefficient of this scale is 0.930. Both scales have a 5-point Likert-type evaluation system.

SPSS 26.0 program was used to analyze the data. Descriptive statistics, reliability analysis, Pearson correlation analysis, simple linear regression analysis, independent sample t-test and one-way analysis of variance (ANOVA) were applied to test differences according to demographic variables. In all statistical analyses, significance level was accepted as $p<0.05$.

III. RESULTS

A. Demographic Characteristics of Participants

The distribution of participants according to gender, age, marital status and professional experience variables is presented in Table I.

Table I. Distribution of Participants According to Demographic Characteristics

Variable	Groups	N	%
Gender	Male	304	84,0
	Female	58	16,0
Age	18-25 years	83	22,9
	26-35 years	106	29,3
	36-45 years	134	37,0
	46 and overyears	39	10,8
Marital Status	Single	142	39,2
	Married	220	60,8
Professional Experience	1-5 years	93	25,7
	6-10 years	152	42,0
	11 and moreyears	117	32,3

The demographic characteristics of the aircraft maintenance personnel included in the study show that male participants (84.0%, n=304) constitute the majority in gender distribution, while female participants are represented by 16.0% (n=58). The age distribution of the participants showed that the highest proportion was in the 36-45 age range (37.0%, n=134). This was followed by the 26-35 age range (29.3%, n=106) and the 18-25 age range (22.9%, n=83). The lowest participation rate was observed in the 46 and over age group (10.8%, n=39). According to marital status data, 60.8% (n=220) of the participants were married and 39.2% (n=142) were single. In terms of professional experience, 42.0% (n=152) of the participants had 6-10 years of experience, 32.3% (n=117) had 11 years or more, and 25.7% (n=93) had 1-5 years of experience.

B. Reliability Analysis

The reliability analysis results of the scales used in the study are presented in Table II.

Table II. Reliability Analysis Results of the Scales

Scale	Number of Items	Cronbach's Alpha
Managerial Support	7	0,823
Employee Creativity	11	0,918

Reliability analysis results show that the Cronbach's Alpha coefficient of the 7-item managerial support scale is 0.823 and the Cronbach's Alpha coefficient of the 11-item employee creativity scale is 0.918. It is seen that both scales are highly reliable and have sufficient internal consistency to collect data suitable for the purpose of the study [8].

C. Normal Distribution Analysis

Skewness and kurtosis values were examined to determine whether the variables used in the study meet the assumption of normal distribution. Normality test results are presented in Table III.

Table III. Normal Distribution Analysis Results

Scale	Skewness	Kurtosis
Managerial Support	-0,662	0,417
Employee Creativity	-0,842	0,738

The analysis revealed that the managerial support variable has -0.662 skewness and 0.417 kurtosis values, while the employee creativity variable has -0.842 skewness and 0.738 kurtosis values. For a normal distribution, it is ideal for these values to be close to zero [13]. In the evaluation made with reference to the ±1.5 interval recommended in the literature [14], it was determined that the assumption of normal distribution was met and parametric tests were decided to be used.

D. Descriptive Statistical Analysis

Descriptive statistical analyses were conducted to determine the measures of central tendency and dispersion for the variables examined in the study. Descriptive statistics are presented in Table IV.

Table IV. Descriptive Statistical Analysis Results

Variable	Mean	sd	Level
Managerial Support	3,88	0,70	High
Employee Creativity	4,07	0,66	High

Considering that the scales used in the study are 5-point Likert type, the score ranges of the scales were cascaded as (5-1)/5=0.80 according to the formula (n-1)/n and classified as very low, low, medium, high and very high, respectively[15]. Table IV shows that aircraft maintenance personnel's perception of managerial support is at a high level ($\bar{x}$=3.88; ss=0.70). Similarly, the level of employee creativity was also found to be at a high level ($\bar{x}$=4.07; ss=0.66). The fact that the standard deviation values of both variables are less than 1 indicates that the participant responses show a relatively homogeneous distribution around the mean. The findings indicate that aircraft maintenance personnel generally evaluate the support they receive from their managers positively and perceive their own creativity level to be quite high.

E. Correlation Analysis

Pearson correlation analysis was conducted to determine the direction and severity of the relationship between the independent variable of the study, managerial support, and the dependent variable, employee creativity. The correlation coefficients and significance levels between the variables are presented in Table V.

TableV. Correlation Analysis Results

Variable	Managerial Support	Employee Creativity
Managerial Support	1	
Employee Creativity	,736**	1

***p<0,01*

Correlation coefficients show negligible relationship levels between 0.00-0.10, weak between 0.10-0.39, moderate between 0.40-0.69, strong between 0.70-0.89 and very strong between 0.90-1.00 [15]. In this framework, Table V shows that there is a positive, strong and statistically significant relationship between managerial support and employee creativity (r=0.736; p<0.01).

F. Regression Analysis

A simple linear regression analysis was conducted to determine the effect of managerial support on employee creativity. The results of the regression model in which managerial support is considered as the independent variable and employee creativity as the dependent variable are presented in Table VI.

TableVI. Results of Simple Linear Regression Analysis

Independent Variable	Dependent Variable	β	t	p
Managerial Support	Employee Creativity	,736	20,625	,000

F=425,323; R2=0,540; p=0,000

The results of the regression analysis show that the model is statistically significant (F=425,373; p<0,001). The R^2 value showing the explanatory power of the model was calculated as 0.540. The R^2 value shows that 54.0% of the variance in employee creativity is explained by managerial support. Studies in the field of social sciences indicate that an R^2 value above 0.50 indicates a high level of explanatory power [13].Regression coefficients indicate that managerial support has a positive and significant effect on employee creativity (β=0.736; t=20.625; p<0.001). The regression coefficient (β=0.736) shows that a one unit increase in managerial support leads to a 0.736 unit increase in employee creativity.

G. Difference Analyses

In this section, the differentiation of the data collected within the scope of the study according to demographic variables is examined. Statistical analyses were conducted to determine whether the levels of managerial support and employee creativity perceived by aircraft maintenance personnel differ significantly according to demographic characteristics such as gender, marital status, age and professional experience. In this context, independent sample t-test was applied for categorical variables with two groups and one-way analysis of variance (ANOVA) was applied for those with more than two groups.

1) Examination of Managerial Support Level According to Demographic Characteristics

In this sub-section, the differentiation of the level of managerial support perceived by aircraft maintenance personnel according to demographic characteristics is discussed.

a) Findings Regarding Gender

Independent sample t-test was conducted to examine whether the level of managerial support perceived by aircraft maintenance personnel working in the aviation sector differs according to gender. The results of the analysis are presented in Table VII.

TableVII. t-Test Results of Level of Managerial Support by Gender

Gender	n	Mean	sd	t	sd	p
Male	304	3,88	0,70	0,421	360	0,674
Female	58	3,84	0,70			

The results in Table VII show that the level of managerial support perceived by aircraft maintenance personnel does not show a statistically significant difference according to gender (t(360)=0.421; p>0.05). The average of male employees' perception of managerial support ($\bar{x}$=3.88; ss=0.70) and female employees' perception of managerial support ($\bar{x}$=3.84; ss=0.70) were quite close to each other.

b) Findings Regarding Marital Status

Independent sample t-test was applied to determine whether the level of managerial support perceived by aircraft maintenance personnel differed according to marital status. The results of the analysis are presented in Table VIII.

TableVIII. t-Test Results of Level of Managerial Support by Marital Status

Marital Status	n	Mean	sd	t	sd	p
Single	142	3,88	0,73	0,065	360	0,948

Married	220	3,87	0,68

The results of the analysis presented in Table VIII show that the level of managerial support perceived by aircraft maintenance personnel does not show a statistically significant difference according to marital status (t(360)=0.065; p>0.05). The mean perception of managerial support of single employees ($\bar{x}$=3.88; ss=0.73) and the mean perception of managerial support of married employees ($\bar{x}$=3.87; ss=0.68) are almost at the same level.

c) Findings Regarding Age

One-way analysis of variance (ANOVA) was applied to determine whether the level of managerial support perceived by aircraft maintenance personnel differed according to age groups. The results of the analysis are presented in Table IX.

TableIX. ANOVA Results of Level of Managerial Support by Age

Age	n	Mean	sd	F	p
18-25 years	83	3,86	0,70	0,442	0,723
26-35 years	106	3,91	0,69		
36-45 years	134	3,83	0,71		
46 and overyears	39	3,95	0,68		

The results of the analysis presented in Table IX show that the level of managerial support perceived by aircraft maintenance personnel does not show a statistically significant difference according to age groups (F(3,358)=0.442; p>0.05). It is seen that employees in the 46 and over age group have the highest mean perception of managerial support ($\bar{x}$=3.95; ss=0.68), while employees in the 36-45 age group have the lowest mean ($\bar{x}$=3.83; ss=0.71). However, the mean perceptions of manager support of all age groups were quite close to each other.

d) Findings Regarding Professional Experience

One-way analysis of variance (ANOVA) was applied to determine whether the level of managerial support perceived by aircraft maintenance personnel differed according to their professional experience. The results of the analysis are presented in Table X.

TableX. ANOVA Results of Managerial Support Level by Professional Experience

Professional Experience	n	Mean	sd	F	p
1-5 years	93	3,87	0,71	1,039	0,355
6-10 years	152	3,93	0,68		
11 and more years	117	3,81	0,72		

The results of the analysis presented in Table X show that the level of managerial support perceived by aircraft maintenance personnel does not show a statistically significant difference according to their professional experience (F(2,359)=1,039; p>0,05). It is seen that employees with 6-10 years of experience have the highest mean perception of managerial support ($\bar{x}$=3,93; ss=0,68) and employees with 11 years of experience and above have the lowest mean ($\bar{x}$=3,81; ss=0,72).

2) Examination of Employee Creativity Level According to Demographic Characteristics

In this sub-section, the differentiation of creativity levels according to demographic characteristics is examined.

a) Findings Regarding Gender

Independent sample t-test was applied to determine whether the level of employee creativity of aircraft maintenance personnel differs according to gender. The results of the analysis are presented in Table XI.

Table XI. t-Test Results of Employee Creativity by Gender

Gender	n	Mean	sd	t	p
Male	304	4,08	0,65	0,591	0,555
Female	58	4,03	0,74		

The results of the analysis presented in Table XI show that the level of employee creativity of aircraft maintenance personnel does not show a statistically significant difference according to gender (t(360)=0.591; p>0.05). The mean creativity level of male employees ($\bar{x}$=4.08; ss=0.65) and the mean creativity level of female employees ($\bar{x}$=4.03; ss=0.74) were quite close to each other.

b) Findings Regarding Marital Status

Independent sample t-test was applied to determine whether the level of employee creativity of aircraft maintenance personnel differs according to marital status. Prior to the analysis The results of the analysis are presented in Table XII.

Table XII. t-Test Results of Level of Employee Creativity by Marital Status

Marital Status	n	Mean	sd	t	sd	p
Single	142	4,02	0,72	-1,216	0,225	4,02
Married	220	4,11	0,62			4,11

The results of the analysis presented in Table XII show that the level of employee creativity of aircraft maintenance personnel does not show a statistically significant difference according to marital status (t(360)=-1,216; p>0,05). There is no significant difference between the mean creativity level of single employees ($\bar{x}$=4.02; ss=0.72) and married employees ($\bar{x}$=4.11; ss=0.62).

c) Findings Regarding Age

One-way analysis of variance (ANOVA) was applied to determine whether the level of employee creativity of aircraft maintenance personnel differed according to age groups. The results of the analysis are presented in Table XIII.

Table XIII. ANOVA Results of Level of Employee Creativity by Age

Age	n	Mean	sd	F	p
18-25 years	83	3,86	0,70	0,442	0,723
26-35 years	106	3,91	0,69		
36-45 years	134	3,83	0,71		
46 and over years	39	3,95	0,68		

The results of the analysis presented in Table XIII show that the level of employee creativity of aircraft maintenance personnel does not show a statistically significant difference according to age groups (F(3,358)=0.442; p>0.05). It is seen that the employees in the age group of 46 and above have the highest mean of employee creativity ($\bar{x}$=3,95; ss=0,68) and the employees in the age group of 36-45 have the lowest mean ($\bar{x}$=3,83; ss=0,71). However, the average employee creativity scores of all age groups were very close to each other.

d) Findings Regarding Professional Experience

One-way analysis of variance (ANOVA) was applied to determine whether the level of employee creativity of aircraft maintenance personnel differed according to professional experience groups. The results of the analysis are presented in Table XIV.

Table XIV. ANOVA Results of Employee Creativity Level by Professional Experience

Professional Experience	n	Mean	sd	F	p
1-5 years	93	3,87	0,70	1,039	0,355
6-10 years	152	3,93	0,69		
11 and more years	117	3,81	0,70		

The results of the analysis presented in Table XIV show that the level of employee creativity of aircraft maintenance personnel does not show a statistically significant difference according to the professional experience groups ($F(2,359)=1,039$; $p>0,05$). It is seen that employees with 6-10 years of experience have the highest mean of employee creativity ($\bar{x}=3,93$; $ss=0,69$) and employees with 11 and more years of experience have the lowest mean ($\bar{x}=3,81$; $ss=0,70$). However, the employee creativity averages of all professional experience groups were quite close to each other.

IV. DISCUSSION

The findings obtained in this study largely overlap with the results of similar studies in the literature. In a study conducted in the chemical industry, similar significant relationships were found [16]. Likewise, positive and significant relationships were found between managerial support and employee creativity in studies conducted in different sectors [17, 18]. In studies using variables similar to managerial support, a positive and significant relationship was found between perceived organizational support and employee creativity [19, 20] and between leader relationship support and employee creativity [21]. Regarding the moderating role of managerial support; in a study conducted in enterprises operating in different sectors in China [22], it was determined that managerial support has a moderating role in the relationship between psychological capital and employee creativity.

The findings regarding demographic variables revealed that the variables of managerial support and employee creativity did not differ significantly according to gender, age, marital status and professional experience groups. These findings are consistent with the results of the studies in the literature [22, 23]. In the mentioned studies, statistically significant relationships were not found between demographic variables (gender, age, tenure, education, job type and sector) and managerial support and employee creativity.

However, the findings of the current study contradict the findings of a study in which professional experience was found to have a moderating effect [17]. In the study, it was revealed that experienced employees were more affected by managerial support and exhibited higher creativity. This difference between the two studies may be due to the cultural characteristics of the samples. Indeed, the study was conducted in Kuwait and the authors emphasized the impact of collectivist culture on results.

From an engineering management perspective, the fact that demographic variables do not show significant differences indicates that managerial support and employee creativity are universal in the aviation industry. This finding of the study can be explained by the industry's standardized processes and high reliability requirements. The fact that demographic characteristics such as gender, age, marital status and professional experience are not determinative indicates that technical competencies and professional standards are at the forefront in the aviation industry.

V. CONCLUSION

This study found that managerial support strongly affects employee creativity in aircraft maintenance organizations (H1 - Accepted), this effect is valid for all employees regardless of demographic characteristics (H2 - Rejected) and both variables are at high levels. The results reveal the importance of managerial support in the aviation industry and indicate that engineering management practices should be shaped accordingly.

In line with the findings of the study, recommendations for practitioners and researchers can be developed. For practitioners, managers in aircraft maintenance organizations can be provided with systematic leadership trainings

covering creative thinking techniques and innovative maintenance practices. Formal mechanisms such as brainstorming meetings and suggestion systems that can evaluate the creative ideas of technical staff can be established and operated effectively. In terms of engineering management, performance appraisal systems can be structured to include criteria that encourage creative thinking. In addition, the regulations of the Directorate General of Civil Aviation can be amended to support the creative potential of technical staff while maintaining safety standards. For future research, comparative studies on the interaction of the relationship between managerial support and employee creativity with variables such as organizational culture and work safety climate can be conducted in aircraft maintenance organizations in different countries.

STATEMENT OF CONTRIBUTION RATE

Authors' contribution rates to the study are equal. / Author contributed 100%.

CONFLICTS OF INTEREST

They reported that there was no conflict of interest between the authors and their respective institutions.

RESEARCH AND PUBLICATION ETHICS

In the studies carried out within the scope of this article, the rules of research and publication ethics were followed.

REFERENCES

[1] Güneş, T., Yılmaz, M. &Karataş, S. (2020). Havacılık bakım organizasyonlarında insan faktörü analizi. *Havacılık ve Uzay Teknolojileri Dergisi*, 13(2), 45-58.
[2] McDonald, N., Corrigan, S., Daly, C., &Cromie, S. (2000). Safety management systems and safety culture in aircraft maintenance organisations. *Safety Science*, 34(1-3), 151-176.
[3] Hobbs, A. & Williamson, A. (2002). Skills, rules and knowledge in aircraft maintenance: Errors in context. *Ergonomics*, 45(4), 290-308.
[4] Rashid, H., Place, S., &Braithwaite, G. R. (2014). Eradicating root causes of aviation maintenance errors: Introducing the AMMP. *Cognition, Technolog yand Work*, 16(1), 71-90.
[5] Köse, S., Mohan Bursalı, Y. & Dolma, S. (2023). Örgütsel adalet ve yönetici desteği ile ihbarcılık arasındaki ilişkide psikolojik güvenliğin aracılık rolü. *Turkish Studies - Economy*, 18(1), 305-325.
[6] Bhanthumnavin, D. (2000). Importance of supervisory social support and its implications for HRD in Thailand. *Psychology and Developing Societies*, 12(2), 155-166.
[7] Karasar, N. (2022). *Bilimsel Araştırma Yöntemleri* (37. baskı). Nobel.
[8] Creswell, J. W& Creswell, J. D. (2022). *Research Design: Qualitative, Quantitative and Mixed Methods Approaches* (6th ed.). SAGE Publications.
[9] AA. (2024). Türkiye'deki pilot sayısı 15 bine yaklaştı. *Anadolu Ajansı*. https://www.aa.com.tr/tr/gundem/turkiyedeki-pilot-sayisi-15-bine-yaklasti/3205938
[10] Karasek, R., Brisson, C., Kawakami, N., Houtman, I., Bongers, P., & Amick, B. (1998). The Job Content Questionnaire (JCQ): An instrument for internationally comparative assessments of psychosocial job characteristics. *Journal of Occupational Health Psychology, 3*(4), 322-355.
[11] Kula, S. (2011). *Occupational stress and work-related wellbeing of Turkish National Police (TNP) members*. Doctoral dissertation, University of Central Florida.
[12] Munoz, M. F., González-Álvarez, N., &Nieto, M. (2008). An examination of individual factors and employees' creativity: Thecase of Spain. *Creativity Research Journal, 20*(1), 21-33.
[13] Hair, J. F., Black, W. C., Babin, B. J., & Anderson, R. E. (2014). *Multivariate Data Analysis* (7th ed.). Pearson Education.
[14] Tabachnick, B. G., &Fidell, L. S. (2013). *Using Multivariate Statistics* (6th ed.). PearsonEducation.
[15] Gürbüz, S., & Şahin, F. (2014). *Sosyal Bilimlerde Araştırma Yöntemleri: Felsefe-Yöntem-Analiz* (2. baskı). Seçkin Yayıncılık.
[16] Çekmecelioğlu, H. G., & Gökkaya, H. (2019). İşin önemi ve yönetici desteğinin bireysel yaratıcılık üzerindeki etkisi. *Kocaeli Üniversitesi Sosyal Bilimler Dergisi*, (37), 195-215.
[17] Zaitouni, M., &Ouakouak, M. L. (2018). Theimpacts of leadership support and coworker support on employee creative behavior. *International Journal of Productivity and Performance Management*, 67(9), 1745-1763.
[18] Zubair, A., Bashir, M., Abrar, M., Baig, S. A. & Hassan, S. Y. (2015). Employee's participation in decision making and manager's encouragement of creativity: The mediating role of climate for creativity and change. *Journal of Service Science and Management*, 8(3), 306-321.

[19] Tang, G., Yu, B., Cooke, F. L., & Chen, Y. (2017). High-performance work system and employee creativity: The roles of perceived organisational support and devolved management. *Personnel Review*, 46(7), 1318-1334.
[20] Akgündüz, Y., Alkan, C. & Gök, Ö. A. (2018). Perceived organizational support, employee creativity and proactive personality: The mediating effect of meaning of work. *Journal of Hospitality and Tourism Management*, (34), 105-114.
[21] Cheung, M. F. Y. &Wong, C. S. (2011). Transformational leadership, leader support, and employee creativity. *Leadership&Organization Development Journal*, 32(7), 656-672.
[22] Cai, W., Lysova, E. I., Bossink, B. A. G., Khapova, S. N., & Wang, W. (2019). Psychological capital and self-reported employee creativity: The moderating role of supervisor support and job characteristics. *Creativity and Innovation Management*, 28(1), 30-41.
[23] Kim, T. Y., Hon, A. H. Y. & Lee, D. R. (2010). Proactive personality and employee creativity: The effects of job creativity requirementand supervisor support for creativity. *Creativity Research Journal*, 22(1), 37-45.

JOURNAL OF SCIENCE, TECHNOLOGY AND ENGINEERING RESEARCH
Bilim, Teknoloji ve Mühendislik Araştırmaları Dergisi
ISSN (Online) 2717-8404
Available *online* at https://dergipark.org.tr/en/pub/jster

RESEARCH ARTICLE

Effect of Triangle Fin Inclination Angle and Aluminum Metal Foam on Melting Process in A Vertical Latent Heat Energy Storage System

[*] Emrehan Gürsoy, [1] Mehmet Gürdal, and [2] Engin Gedik

[*]Kardemir Karabük Iron Steel Industry Trade & Co. Inc., Karabük, Türkiye
emrehangursoy@gmail.com, Orcid.0000-0003-2373-3357
[1]Department of Mechanical Engineering, Kastamonu University, Kastamonu, Türkiye
mgurdal@kastamonu.edu.tr, Orcid.0000-xxx-0003-2209-3394
[2]Department of Mechanical Engineering, Kastamonu University, Kastamonu, Türkiye
egedik@karabuk.edu.tr, Orcid.0000-xxx-0002-3407-6121

Citation:
Gursoy, E., Gurdal, M., Gedik, E. (2025) *Effect of Triangle Fin Inclination Angle and Aluminum Metal Foam on Melting Process in A Vertical Latent Heat Energy Storage System*, Journal of Science, Technology and Engineering Research, (6):1, 11-30.DOI: 10.53525/jster.1635055

HIGHLIGHTS

- *Effect of triangles fin structure on melting and energy storage performance has been investigated.*
- *MF significantly changed the natural convection behavior in the LHTES.*
- *87.5 times reduction is realized in the melting time because of MF.*
- *In the analyzed systems, stored energy of 54.83 kJ.m^{-1} is achieved.*

Article Info

Received: February 7, 2025
Accepted: February 19, 2025

DOI: 10.53525/jster.1635055

***Corresponding Author:**
Emrehan Gürsoy
emrehangursoy@gmail.com
Phone: +90 535 687 1526

ABSTRACT

The main objective of this numerical study is to investigate the effect of triangle fin inclination angles (IAs) on the melting process in a Latent Heat Thermal Energy Storage (LHTES) system designed as a vertical rectangular cavity with and without metal foam (MF). In the cases, paraffin wax phase change material (PCM) filled the entire domain, and the Brinkman-Darcy-Forchheimer model, assuming local thermal equilibrium (LTE), and the enthalpy-porosity method were employed to simulate the melting process. In total, 14 different cases were analyzed and the results were validated with literature at high accuracy. Melting time, stored energy, temperature variation, and hydrodynamical behavior of the melting derived from numerical simulations are provided. The findings highlight that utilizing MF has reduced the melting time by 87.5 times and it provided a uniform melting due to enhancing the thermal conductivity of the domains. Also, MF has varied melting behavior and the shortest melting time was realized at 120° without MF, while cases with MF experienced the earliest melting at R-60°. However, using MF decreased the stored energy amount at the rate of 5.69% while the highest energy storage was realized without MF of R-60° as 54.83 kJ.m^{-1}.

Keywords: *Latent heat thermal energy storage; Melting; Metal foam; Phase change material; Triangle fin.*

I. INTRODUCTION

The increasing global temperature and the ongoing climate crisis are widely recognized challenges. In response, 175 nations have committed to the Paris Agreement, aiming to reduce greenhouse gas emissions by 45% by 2030 and achieve net-zero emissions by 2050. Despite these commitments, the International Energy Agency's 2023 report reveals that 80% of global energy consumption is still derived from non-renewable sources, highlighting a significant gap between current efforts and energy demands. To address this disparity, greater emphasis must be placed on the research and development of renewable energy technologies. However, renewable energy sources such as solar and wind are inherently limited by variability in weather, seasonal changes, and time of day. To mitigate these challenges, advanced energy storage systems, including batteries, thermal energy storage (TES), pumped hydro storage, flywheel energy storage, compressed air energy storage, hydrogen energy storage, and supercapacitors, have been developed. Recent advancements in these technologies demonstrate significant progress, suggesting their growing potential to support renewable energy integration.

TES plays a crucial role in balancing the supply and demand of energy, particularly in optimizing intermittent energy sources like solar thermal systems. Among the various TES approaches, LHTES offers a promising alternative to conventional sensible heat storage systems due to its higher energy density potential. LHTES typically utilizes solid-liquid PCMs, which store or release energy at a constant temperature, known as latent heat. These materials are advantageous because of their narrow temperature range, cost-effectiveness, reusability, and ease of integration into thermal systems. Furthermore, they demonstrate significantly higher energy storage densities compared to sensible heat storage fluids such as oil, air, or water. However, one of the key challenges of PCMs is their low thermal conductivity, which significantly impacts system performance [1]. Consequently, various strategies have been developed to enhance their heat transfer capabilities.

Choure et al. [2] categorized techniques to improve the thermal conductivity of PCMs into four main groups: a) the use of high thermal conductivity materials, b) modification of geometry, c) incorporation of multiple phase change materials, and d) the integration of fins with various shapes. Among these, the use of MF, which falls under the first category, is particularly prominent due to its high thermal conductivity, large heat transfer surface area, and low thermal resistance. For instance, Liu et al. [3] explored both experimentally and numerically the effect of non-uniform MF embedded in PCM to mitigate the negative impacts on solar systems and improve solar energy utilization. Their study demonstrated that natural convection accelerated the PCM melting process and inhibited solidification. The optimal conditions for PCM melting and solidification were found to be in the range of $\varepsilon = 0.94$ with specific porosity values for each process. Notably, reductions of 9.7% and 6.2% in the consumption time for melting and solidification processes, respectively, were observed. Liu et al. [4] conducted a study on LHTES using multiple PCMs and MF structures showed significant improvements in thermal performance. The key quantitative findings show that the use of multiple PCMs reduced the complete melting time by 9.18% compared to a single PCM with uniform MF. A one-dimensional positive porosity gradient reduced the melting time by 6.18%, while a negative gradient increased it by 19.78%. On the other hand, the optimal two-dimensional porosity gradient multi-PCM storage system reduced the complete melting time by 17.96% and increased energy storage efficiency by 20.16% compared to the single PCM system with uniform porosity.

The study published by Xing et al. [5] investigated the use of water embedded in copper MF to enhance TES performance, both numerically and experimentally. The effects of the filling ratio, MF specification, and arrangement on heat transfer during the solidification/melting process were analyzed. Results indicated that as the filling ratio increased from 0 to 6.6%, the cold storage/release rate and overall heat transfer coefficient increased, while thermal cycle time, supercooling, and cold storage/release capacity decreased. Notably, heat conduction increased from 67.72% to 91.22% as the filling ratio rose from 3.2% to 6.6%, indicating that heat conduction dominates at higher filling ratios. Yang et al. [6] highlighted significant advancements in LHTES by incorporating graded MFs and active flipping methods to enhance heat transfer and mitigate the low thermal conductivity of PCMs. Key findings reveal that optimal thermal performance occurs at a 6% porosity gradient and a dimensionless flipping time of 0.4, reducing melting time by 49.37% and improving the thermal energy storage rate by 76.23%. Shen et al. [7] employed a solid-

liquid lattice Boltzmann model at the REV scale to examine how gradient porosity enhances LHTES. Among three gradient porosity configurations-Chinese-fan-shape, vertical, and concentric-the fan-shape arrangement delivers the best performance, reducing melting time by 36.1% compared to homogeneous porosity while achieving better temperature uniformity. Increasing the number of layers beyond two yields minimal improvements in melting time (up to 4.4%), whereas higher porosity gradients significantly increase melting time by at least 36.1%. Alasmari et al. [8] investigated the role of a 30% MF layer in enhancing heat transfer in LHTES systems on both the heat transfer fluid side and the shell side. Using a two-temperature heat equation model and finite element analysis, the research reveals that optimizing the MF layer's position and shape parameter (FL) can significantly reduce melting time by approximately 40%. At an inlet pressure of 750 Pa, increasing the FL parameter from 0.75 to 1.37 raises energy storage power during 90% charging from 32.2 W to 48.7 W, marking a 34% improvement. These findings highlight the potential of MF integration for improved thermal performance in LHTES systems. Bouzidi et al. [9] explored the application of anisotropic MF with tailored local characteristics to enhance heat transfer in LHTES. Unlike previous research on partial MF, this work integrates heterogeneous copper foam into a shell-tube system with paraffin wax, analyzing various heterogeneity angles (-90° to 90° in 15° increments) using finite element methods. Results reveal that the most effective configuration, with a 0° heterogeneity angle, reduces charging and discharging times to 623 and 989 minutes, respectively, compared to 646 and 1007 minutes for uniform MF.

Ahmed et al. [10] experimentally evaluated the heat storage properties of PCMs enhanced with copper and iron-nickel MFs. The thermal behavior of paraffin within these composites is compared to pure paraffin under a constant heat flux of 1000 $W.m^{-2}$ across three directions. Results show that incorporating MFs significantly improves thermal conductivity, with copper MF/paraffin composites achieving superior temperature uniformity compared to iron-nickel MF/paraffin composites and pure paraffin. Notably, the copper MF/paraffin composite reduces heat storage time to 20.63% of the time required by the iron-nickel MF/paraffin composite, highlighting its efficiency in enhancing thermal performance. Nassar et al. [11] aimed to enhance the low thermal conductivity of conventional PCMs by investigating composites with MFs and hybrid nanoparticles. Results indicate that increasing the weight percentage of MF and nanoparticles improves thermal conductivity, achieving a 37.7% enhancement for copper-based composites. The optimal specific surface value of 1600 $m^2.m^{-3}$ delivers superior thermal performance. While increased MF content also enhances heat capacity, the fixed shapes of MFs pose challenges in compatibility with PCM formability, limiting their use in compact applications. Liu et al. [12] conducted a pore-scale numerical analysis of PCM melting in a truncated cuboctahedron (TCD) and tetrakaidecahedron (TKD) MF. Results reveal that natural convection reduces melting time by about 7% within the examined porosity range. The TCD MF accelerates melting in the early stage due to its larger surface area, while the TKD MF is more effective in the later stage due to thicker metallic ligaments. A critical porosity threshold determines which structure provides superior enhancement, shifting from TCD to TKD as porosity decreases. At porosity of ε=0.941, both foams yield similar total melting times, but half-melting occurs faster in TCD (17.2%) compared to TKD (20.3%), highlighting structural influence on phase transition dynamics.

Du et al. [13] investigates the enhanced heat transfer properties of MF in a LHTES system. A 3D transient numerical model of a horizontal square cavity LHTES unit is developed to analyze the impact of MF on melting and solidification processes. An experimental LHTES system is constructed for model validation. The Taguchi method is used to evaluate the effects of MF porosity (ε) and pore density (ω) on phase transformation, heat charging, and discharging times. Results indicate that MF porosity has a greater impact on the phase transformation process than pore density. For example, the melting-solidification time of Case 3 (ε=0.97, ω=30 PPI) is 67.46% shorter than that of Case 9 (ε=0.99, ω=30 PPI). Additionally, Case 3 shows a 199.33% increase in heat charging efficiency and a 196.35% improvement in heat release efficiency compared to Case 9.

The number of studies investigating the effect of fin types on LHTES performance shows an increment in the last years. Within this scope, Moaveni et al. [14] conducted a study on the thermal management of lithium-ion batteries under maximum performance and safety conditions. Their findings showed that adding nanoparticles (φ =

9.0%) and using four fins reduced the peak temperature by 5.18K and 10.36K at a 4C discharge rate, respectively. Additionally, the application of copper MF (ε=0.90) reduced the temperature by 12.57K at a 3C discharge rate. The study carried out by Yang et al. [15] on LHTES using solid-liquid PCM found that the optimal configuration of finned MF with graded porosity significantly improves thermal performance. Specifically, compared to the base case, this configuration shortens melting time by 46.68%, increases the TES rate by 74.06%, and increases the Nusselt number by 69.02%. Besides, the optimal parameters have been acquired as a fin length of 20 mm, a fin width of 1.5 mm, a porosity gradient of 2%, and a rotational speed of 0.5 rpm. A novel staggered fin-foam design is proposed by Lu et al. [16] to assess the impact on melting performance in shell-and-tube. The straight fin-foam configuration reduces melting time by 58.67% compared to foam-only designs. Further improvements are seen with a segmented staggered configuration, with the optimal design (four segments) reducing melting time by an additional 13.18%. This configuration enhances heat transfer and lowers the outlet temperature by 23.55 K, improving heat utilization. Rahmanian et al. [17] examined the various LHTES systems with different MF fin configurations that were simulated and compared to pure PCM and fully MF enclosures. Two boundary conditions, constant temperature, and constant heat flux, were considered. Results showed that MF fins significantly improved thermal performance under constant temperature conditions. For systems with six MF fins, melting times were reduced by 42% and 30% under constant temperature and heat flux conditions, respectively. Additionally, the input heat rate was enhanced by up to 112% and 155% for systems with 6 MF fins and fully MF configurations, respectively.

Hasan et al. [18] investigated the impact of two fin configurations, I-shaped and V-shaped, on the solidification process of a paraffin-based PCM loaded with CuO nanoparticles. The configurations were designed to maintain the same volume of paraffin. Numerical simulations using the Finite Volume Method (FVM) and an implicit technique revealed that the system with I-shaped fins required 8.93% less time for solidification than the V-shaped fins. The freezing times were 47.26 minutes for the I-shaped fins and 51.89 minutes for the V-shaped fins, indicating that the I-shaped fins enhanced solidification performance. Zhang et al. [19] studied the heat transfer mechanisms in shell-and-tube and annular finned shell-and-tube latent TES systems. They discovered that both convection and heat conduction are key to the heat transfer process in the annular finned shell-and-tube TES. However, natural convection led to uneven melting, affecting liquid fraction and temperature uniformity. To better utilize natural convection during the melting process, several innovative annular fin configurations have been proposed in the literature. Abhinand S et al. [20] explored the melting behavior in a LHTES using ice as the PCM and fins to enhance thermal performance. The research aims to determine the optimal number of fins to improve heat transfer and minimize melting time in the tube. Various parameters, such as tube arrangement, diameter, and temperature, were evaluated for their impact on charging performance. The findings show that increasing the number of fins from 4 to 15 boosts the generated liquid PCM by 34.69%, with a subsequent decrease of 9.03% beyond 15 fins. A staggered tube arrangement improves melting performance compared to an inline arrangement. Additionally, a higher tube temperature (280 K) produced 2.08 times more liquid PCM than at 275 K, and increasing the tube diameter from 5 mm to 20 mm enhanced the charging process, generating 2.68 times more liquid PCM.

Fahad et al. [21] investigated the impact of six modified longitudinal fin designs in a shell-and-tube heat exchanger unit on the charging and discharging of PCM. The designs include modifications to the traditional rectangular fin shape (Case 1), with variations such as tapering (Case 2), inverse tapering (Case 3), herringbone wavy (Case 4), convex (Case 5), and constricted (Case 6) shapes. The performance of the designs was assessed based on the total phase transition time, melting time, and solidification time. Case 4, with the herringbone wavy shape, showed the best performance, improving total phase transition time by 10.93%, melting time by 8.48%, and solidification time by 12.31% compared to the traditional rectangular fin. Conversely, Case 5, the convex shape, performed the worst, with decreases of 3.55%, 5.88%, and 5.04% in total cycle time, melting time, and solidification time, respectively, compared to the base case. Farahani et al. [22] examined the numerical analysis of heat transfer and PCM melting enhancement in a three-dimensional cylindrical LHTES system using RT82 as the PCM. The study investigates the effects of strip fins, Fe_3O_4 nanoparticles, and both uniform and non-uniform magnetic fields on PCM melting. The results show that the introduction of strip fins reduces the PCM melting time by approximately 51%

compared to no fins. Abdulrazzaq et al. [22] focused on improving the performance of PCM-based shell-and-tube LHTES systems by utilizing differently shaped fins. PCM systems face challenges due to their low thermal conductivity, which this study addresses by incorporating conductive fins. The system consists of concentric cylinders, where the inner cylinder carries the heat transfer fluid and the outer one contains the PCM. Four different fin shapes (straight, curved, and wavy) are attached to the heat transfer fluid cylinder. The results indicate that the use of a curved fin reduces the melting time by 122.2% compared to the no-fin case. The findings demonstrate that modifying the geometry of the system significantly enhances the heat energy storage rate, offering valuable insights for designing more efficient and compact thermal energy storage systems. Ao et al. [23] explored the enhancement of heat transfer efficiency in LHTES units using novel three-tube heat exchangers with longitudinal fins. The research investigates the impact of fin number, length, thickness, and arrangement on the melting performance of PCM. The results show that thinner and longer fins significantly reduce the melting time, with the complete melting time of thin long fins being 10.6% faster than short thick fins. The optimal fin length was found to be 30 mm, which shortened the heat storage time by 18%. Additionally, a lower long and upper short fin arrangement improved heat transfer efficiency. Du et al. [24] compared the heat storage and release performances of four structures: pure paraffin, fins, MF, and fin-MF, throughout the complete melting-solidification cycle. Using experimental snapshots and real-time data acquisition, the study evaluates phase interface changes and internal temperature variations. Results show that both fins and MF improve melting and solidification, with fins offering better temperature responses and MF providing greater temperature uniformity. The combination of fins and MF demonstrates the best heat storage/release performance, reducing heat storage and release time by 61.6% and 82%, respectively, and improving average temperature response by 122.4% and 429.8% compared to pure PCM.

Huang et al. [25] used numerical analysis to investigate heat storage and release in a square LHTES unit, enhanced by fins, MF, and a periodic sinusoidal heat source. An experimental setup validates the numerical findings, and the Box-Behnken design in response surface methodology is used for optimization. The results show that fin position and MF pore density do not impact the PCM volume. The initial design with evenly spaced fins creates a refractory zone during phase transformation, with temperature fluctuations due to heat source instability. Optimal results indicate that increasing transverse fin spacing reduces total storage-release time, while increasing longitudinal fin spacing and pore density initially decreases and then increases storage-release time. The optimal structure achieved a 29.55% reduction in total storage-release time, a 20.74% increase in average heat storage rate, and a 65.75% increase in heat release rate during solidification compared to Case 1.

Zeng et al. [26] introduced a novel fin-MF combination to enhance melting and solidification in horizontal shell-and-tube latent heat storage devices. Upward fins accelerate natural convection, while downward foams improve thermal conduction. Numerical analysis compares this design with typical eccentric and concentric configurations throughout the full phase change cycle. The fin-MF combination achieves the best performance, reducing melting time by 47.9% and solidifying time by 55.4%, while minimizing the "buckets effect" in eccentric designs by lowering the melting-solidifying time difference to 12%. The existing literature indicates that numerous studies have explored the heat transfer characteristics of LHTES systems enhanced by MF under various conditions, including natural convection. However, further investigation is needed regarding the specific impact of triangular fin structures and their varying IAs in the context of PCM-MF hybrid systems. Such systems have potential applications in a wide range of fields, including solar energy systems [27], microelectronics [28], and building thermal management [29].

Building on this gap in the literature, the present study examines in detail the heat transfer, heat storage, and melting performance of triangular-finned rectangular cavities filled with PCM and embedded with MF. A numerical study has been conducted to explore the effects of triangular fin IAs, along with the presence of tending and aluminum-based MF, under laminar flow and natural convection conditions.

II. MODEL DESCRIPTION

A two-dimensional schematic representation of the computational domain is illustrated in Figure 1. The domain consists of a rectangular cavity with dimensions of 30 mm in height (H) and 10 mm in width (W). It is filled alternately with pure PCM and PCM combined with MF to compare cases with and without MF structure. The left wall of the domain is maintained at a constant temperature of 335.15 K, while the remaining walls are treated as adiabatic with no-slip conditions. The initial temperature across the domain is set at 298.15 K. The top wall features a triangular geometry, with IAs varying along its length from left to right. This study aims to analyze heat transfer behavior within the PCM during the melting process when encountering obstacles. Rubitherm RT58 paraffin wax, an organic PCM, was selected for the study. The MF, assumed to be aluminum, was characterized by a porosity of ε=0.9 and a pore density of ω=20 PPI.

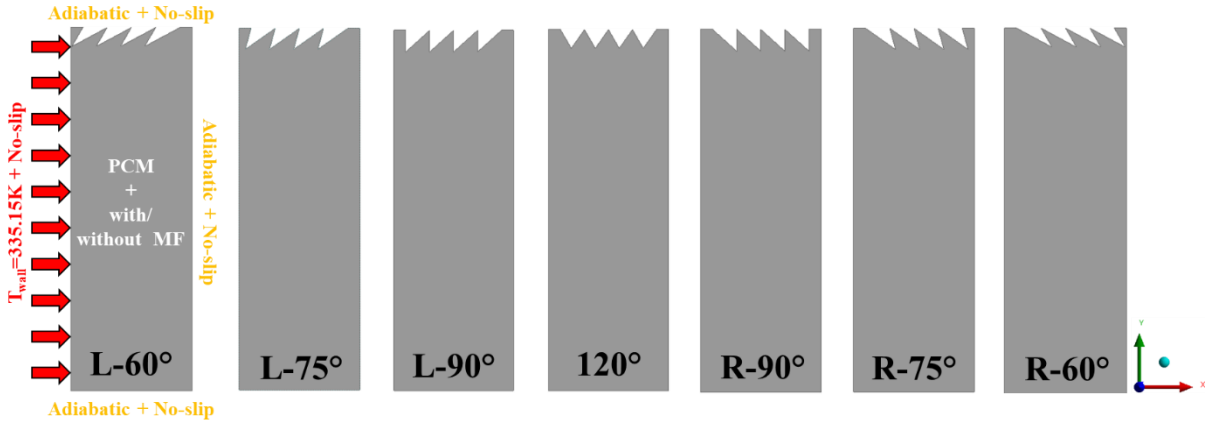

Figure 1. Schematic view and boundary conditions of the computational domain.

The Forchheimer-extended Darcy model has been utilized to simulate heat transfer between the PCM and MF, incorporating the LTE hypothesis. This hypothesis assumes that the time-averaged internal temperatures of the fluid and solid phases are equal, with supporting studies in the literature validating its applicability for aluminum MF with a ω=20 PPI [30], [31]. The study operates under the following assumptions:

i. The liquid phase of the PCM behaves as a Newtonian and incompressible fluid.
ii. Except for density, the thermophysical properties of both the PCM and MF remain constant regardless of the phase change.
iii. The Boussinesq approximation is applied to account for density variations due to buoyancy effects in the momentum equation, given the small temperature differences.
iv. The MF is considered homogeneous and isotropic in all directions.
v. The domain volume is assumed to remain constant throughout the melting process.

The governing equations for the PCM and MF combination are provided below, derived from the stated assumptions and hypotheses. The enthalpy-porosity method is employed to model the melting process.

This approach does not explicitly track the melt interface; instead, it assigns a liquid fraction to each cell within the computational domain. This fraction quantifies the proportion of the cell volume that exists in the liquid state and is determined iteratively using an enthalpy balance [32]. Based on this methodology, the continuity equation is expressed as shown in Eq. (1) [33].

$$\nabla \cdot V = 0 \tag{1}$$

where V denotes the velocity field within the computational domain. The momentum equation, which governs the fluid motion, is provided in Eq. (2) [34].

$$\frac{\rho_p}{\varepsilon}\frac{\partial V}{\partial t}+\frac{\rho_p}{\varepsilon^2}V\cdot\nabla V = -\nabla P+\frac{\mu_p}{\varepsilon}\nabla^2 V-\frac{(1-\beta)^2}{(\beta^3+0.001)}A_{mush}V-\left(\frac{\mu_p}{K}V+\frac{C_F}{\sqrt{K}}\rho_p V|V|\right)+\rho_p g\gamma\Delta T_0 \quad (2)$$

in which ρ_p [kg.m^{-3}], μ_p [Pa.s], and γ [K^{-1}] describe the density, dynamic viscosity, and thermal expansion coefficient of PCM, respectively. Furthermore, ε, β, A_{mush} [kg.m^{-3}.s^{-1}], C_F [m^{-1}], g [m.s^{-2}], ΔT_0 [K], K [m^2], and P [Pa] show the porosity of MF, liquid fraction, mushy constant (set to 10^5 kg.m^{-3}.s^{-1}),

Forchheimer drag (inertial) coefficient, gravity (set to 9.81 m.s^{-2}), the temperature difference relies on the Boussinesq approximation, permeability, and pressure. The energy equation written in Eq. (3) is considered due to the LTE hypothesis [33].

$$(\rho c)_{eff}\left(\frac{\partial T}{\partial t}+V\cdot\nabla T\right)=k_{eff}\nabla^2 T-\varepsilon\rho_p H_L\frac{\partial\beta}{\partial t} \quad (3)$$

The term k_{eff} [W.m^{-1}.K^{-1}], as defined in Eq. (4), represents the volume-averaged effective thermal conductivity within the fluid and MF region, while H_L [J.kg^{-1}] denotes the latent heat of the PCM [32].

$$k_{eff}=\varepsilon k_{PCM}+(1-\varepsilon)k_{MF} \quad (4)$$

The terms in the momentum equation related to MF need to be defined using validated mathematical expressions. To achieve this, the permeability of the MF is determined using Eq. (5) [35].

$$K=\frac{\varepsilon^2 d_k^2}{36\,(\delta^2-\delta)} \quad (5)$$

The parameters d_k [m] and δ represent the characteristic length and the tortuosity coefficient of the MF, respectively. These parameters are defined using Eqs. (6) and (7) [35].

$$d_k=\frac{\delta}{3-\delta}d_p \quad (6)$$

$$\delta=2+2\cos\left[\frac{4\pi}{3}+\frac{1}{3}\cos^{-1}(2\varepsilon-1)\right] \quad (7)$$

The Forchheimer's drag (inertial) coefficient is determined using Eq. (8) [35].

$$C_F=0.00212(1-\varepsilon)^{-0.132}\left(\frac{d_f}{d_p}\right)^{-1.63} \quad (8)$$

The parameters d_f [m] and d_p [m] represent the fiber diameter and pore diameter of the MF, respectively, and can be calculated using Eqs. (9) and (10) [35].

$$d_f = 1.18\sqrt{\frac{1-\varepsilon}{3\pi}}\left(\frac{1}{1-e^{\left(-\frac{1-\varepsilon}{0.04}\right)}}\right) \tag{9}$$

$$d_p = \frac{0.0254}{\omega} \tag{10}$$

The pore density, ω [PPI], is specified as 20 PPI. In solidification and melting phenomena, one of the critical parameters is the liquid fraction (β). This parameter, incorporated into the momentum equation (Eq. (2)), varies within the range $0 \leq \beta \leq 1$ based on the solidus and liquidus temperatures. Consequently, the equation describing the variation of β is provided in Eq. (11) [35].

$$\beta = \frac{\Delta H}{H_L} = \begin{cases} 0 \; if \; T < T_S \\ \dfrac{T - T_S}{T_L - T_S} \quad if \; T_S < T < T_L \\ 1 \; if \; T > T_L \end{cases} \tag{11}$$

T_S [K], T_L [K], and T [K] represent the solid phase temperature, liquid phase temperature, and local temperature, respectively. Additionally, β depends on the local temperature (T), with PCM starting to melt when T exceeds T_S. The variation in enthalpy, which reflects the stored energy, can be determined using Eqs. (12)-(14) [33].

$$\Delta H = \Delta H_{PCM} + \Delta H_{MF} = \varepsilon \int (\rho \Delta h)_{PCM} dA + (1-\varepsilon) \int (\rho \Delta h)_{MF} \, dA \tag{12}$$

$$(\rho \Delta h)_{MF} = c_{p_{MF}}(T_{MF} - T_{in}) \tag{13}$$

$$(\rho \Delta h)_{PCM} = \begin{cases} c_{p_{PCM,S}}(T_{PCM} - T_{in}) \; if \;\; T_{PCM} < T_S \\ c_{p_{PCM,S}}(T_s - T_{in}) + H_L \beta \; if \;\; T_S < T_{PCM} < T_L \\ c_{p_{PCM,S}}(T_S - T_{in}) + H_L + c_{p_{PCM,L}}(T_{PCM} - T_L) \; if \; T_L < T_{PCM} \end{cases} \tag{14}$$

in which ΔH_{PCM} and ΔH_{MF} represent the enthalpy variations of the PCM and the MF, respectively, while their sum constitutes the total enthalpy variation (ΔH) of the TES system. Additionally, h, A, and T_{in} denote the specific enthalpy, volume, and initial temperature of the TES system, respectively. In the analyses, RT58 (Rubitherm) has been used as the PCM, and aluminum MF has been selected for the study. The thermophysical properties of these materials are listed in Table 1.

Table 1. Thermophysical properties of RT58 PCM and aluminum MF [33].

Properties	RT58	Aluminum
Density, ρ [kg.m^{-3}]	825	2719
Specific heat, c_p [J.kg^{-1}.K^{-1}]	2000	871
Thermal conductivity, k [W.m^{-1}.K^{-1}]	0.2	202.4
Dynamic viscosity, μ [kg.m^{-1}.s^{-1}]	0.0269	-

Thermal exp. coeff., γ [K^{-1}]	0.00011	-
Latent heat, H_L [$J.kg^{-1}$]	160000	-
Solidus temperature, T_s [K]	326	-
Liquidus temperature, T_L [K]	332	-

Following the critical information outlining the problem under investigation, the solution methodology for the numerical analysis is defined. The analyses were performed using ANSYS Fluent 2024 R1 software, which employs the FVM for calculations. The pressure-velocity coupling was resolved using the SIMPLE algorithm and its prefer to increase the robustness and efficiency handling incompressible flow and strong coupling between temperature, velocity, and pressure fields [36]–[38]. The SIMPLE algorithm ensures proper pressure-velocity coupling by iteratively correcting velocity fields, which is essential for conserving mass in phase change processes [39]. It effectively handles low-speed buoyancy-driven flows, stabilizing the pressure and velocity fields in transient melting/solidification problems [40]. Pressure was calculated with the PRESTO algorithm because its superior accuracy in handling pressure gradients in the case with strong body force including natural convection-driven phase change [41]. The PRESTO! scheme enhances pressure interpolation, reducing numerical artifacts like checkerboarding and improving pressure gradient resolution. Since phase change is often accompanied by natural convection, PRESTO! provides higher accuracy in buoyancy-driven flows by refining the pressure field distribution [42].

By combining SIMPLE and PRESTO!, software achieves greater numerical stability and physical realism in melting process, ensuring reliable predictions of phase change dynamics. Besides, under-relaxation factors were set as 0.3 for pressure, 1.0 for density, 0.7 for momentum, 0.9 for liquid fraction, and 1.0 for energy. Additionally, the convergence criteria were established as 1×10^{-6}, 1×10^{-5}, and 1×10^{-6} for continuity, momentum, and energy, respectively.

To evaluate the effects of mesh density and time step size, convergence and sensitivity analyses were performed for the case of 120° including MF. The fluid domain was discretized into small volume cells using local mesh settings, independent of mesh quality metrics. A mesh convergence analysis was conducted for three different mesh densities. The quality metrics, specifically the minimum orthogonal quality, and maximum skewness, were maintained approximately constant at 0.730 and 0.528, respectively.

As illustrated in Figure 2(a), the liquid fraction remains unaffected by varying mesh densities, with a maximum error rate of 0.2% observed compared to the 19400-mesh number. These results indicate that the mesh density does not significantly influence the results. Consequently, the mesh configuration with the 7500-mesh number was selected for further analysis, and its schematic structure is shown in Figure 3. Additionally, a time step sensitivity analysis was performed for t=0.1, 0.5, and 1.0s using the 7500-mesh number configuration. According to Figure 2(b), the trends in the liquid fraction are consistent across all time steps. The maximum error rates in liquid fraction between t=0.1s and t=0.5s, as well as t=0.1s and t=1.0s, were 3.23% and 7.08%, respectively. Based on these findings, t=0.5s was selected as the optimal time step for subsequent analyses.

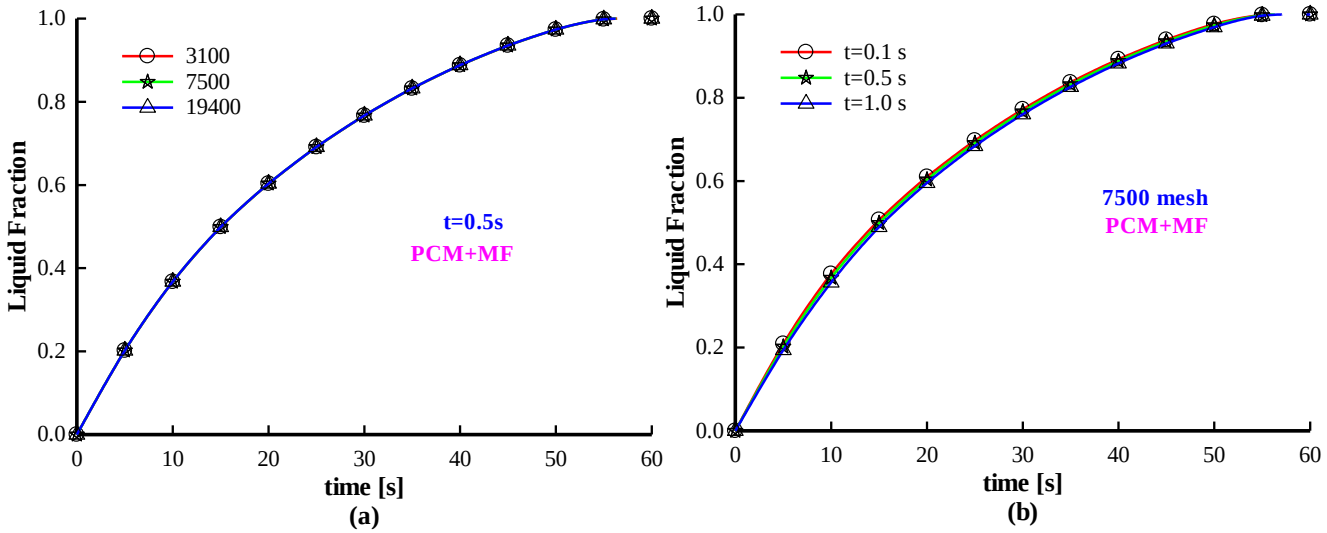

Figure 2. Variation of liquid fraction for; (a) mesh convergence analysis at t=0.5s and (b) time step sensitivity analysis for 7500 mesh number.

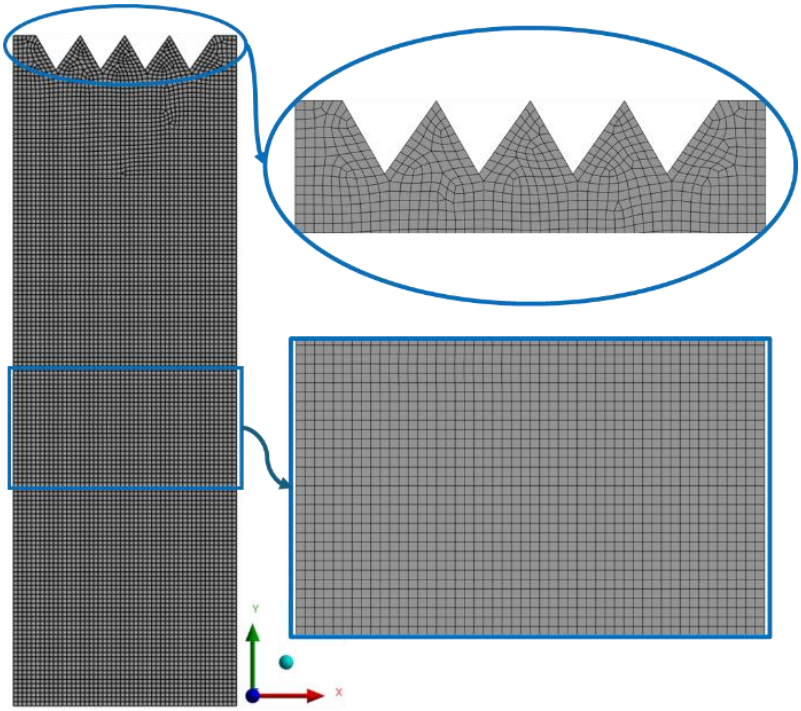

Figure 3. Presenting of the mesh structure with 7500 mesh numbers.

To validate the accuracy of the methods and solutions applied in the numerical study, a validation analysis was performed using data from the literature. The comparative analysis was based on the work of Huang et al. [35] focusing on the liquid fraction in a fluid domain without a fin structure. In order to perform the validation, an exact copy of the study conducted by Huang et al. was designed. The suitability of the mesh study and the selected solution methods was tested in this way. To obtain a complete replica solution data, a vertical rectangular cavity without triangular fins was created and heated with 335.15K from one wall. The other walls were assumed to be adiabatic and no-slip condition was assumed on all walls. A copper MF with porosity and pore density of ε=0.90 and ω=10 PPI, respectively, was placed inside the rectangular cavity and the entire volume was filled with RT42 PCM. The results of the current study were compared with the reference data, as shown in Table 2 and Figure 4, respectively, considering the liquid fraction.

The comparison revealed that the contours demonstrated a high degree of similarity, confirming the reliability of the numerical approach. Besides, liquid fraction trends show a high harmony between each other, and the average deviation has been acquired as 0.83%.

Table 2. Validation of the numerical solution methods via liquid fraction contours as a function of time.

Time, t [s]	60	180	360	540	720	900
Huang et al. [35]						
Present study						

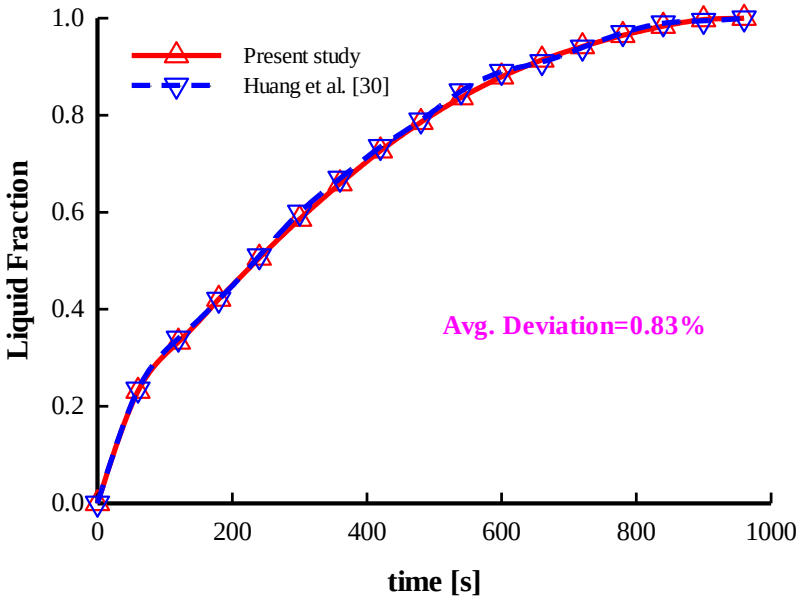

Figure 4. Validation of the numerical solution methods via liquid fraction trends as a function of time.

III. RESULTS AND DISCUSSIONS

The changing of liquid fraction as a function of time is presented in Figure 5 for PCM and PCM+MF cases. Presenting liquid fraction results is critical to understanding heat transfer processes and system performance. A logarithmic growth is seen both each case with increasing time. As the figures examined, LHTES of 120° first reached the full liquid phase on condition including only PCM. Initially, entire cases performed similar melting characteristics. However, 120° provided a considerable difference between the time of t=437.5-2625s compared to other cases, and the difference in melting rate reached up to 15.0% in this period. On the other hand, utilizing MF has accelerated the melting due to increasing the effective thermal conductivity. Also, MF has changed the melting characteristics and the R-60° configuration provided the full liquid phase condition, primarily. The reason for this situation can be attributed to the homogenous behavior of the MF.

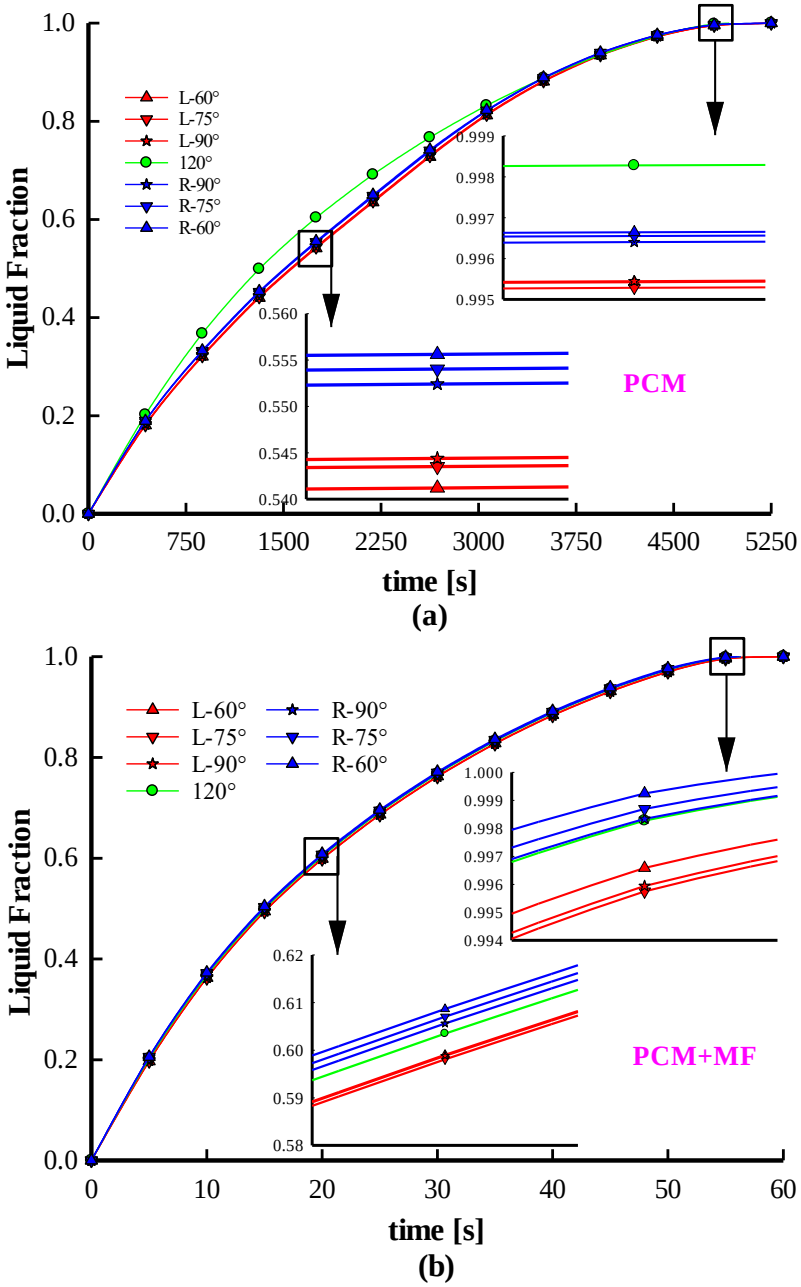

Figure 5. Liquid fraction versus time considering different IAs for; (a) without MF and (b) with MF.

The melting behavior of the LHTES with 120° and R-60° has been visually presented in Table 3. It was concluded that the presence of MF significantly influenced the system's behavior. Specifically, in the absence of MF, the 120° configuration exhibited the highest melting performance. Conversely, in the presence of MF, the R-60° configuration achieved the highest melting performance. Additionally, the liquid fraction of the PCM embedded within MF was found to be more uniformly distributed compared to the PCM without MF. In the case of without MF, natural convection is more dominant than heat conduction. At t=875s, heat mostly progresses with the help of conduction. However, the effect of buoyancy force increased melting behavior progressively and the melted PCM on the bottom side of the rectangular cavity carried out the upper side. Because of this, a natural convection can be observed after the t=875s, and a logarithmic solid-liquid interface is seen at the upper side. In the case of including MF, there is no logarithmic solid-liquid interface and the melting progressed linearly from the left side to the right side because heat conduction is more dominant than natural convection.

Table 3. Comparison of liquid fraction contours belonging to 120° and R-60° LHTES configurations.

Without MF				
Time, t [s]	**875**	**2187.5**	**3500**	**4812.5**
120°	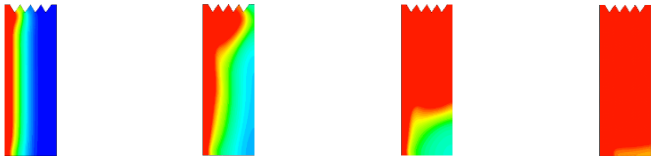			
R-60°	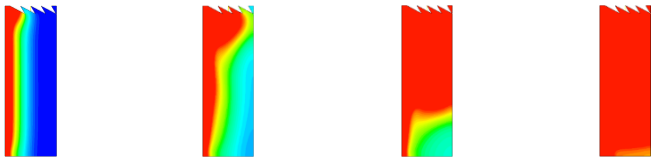			
With MF				
Time, t [s]	**10**	**25**	**40**	**55**
120°	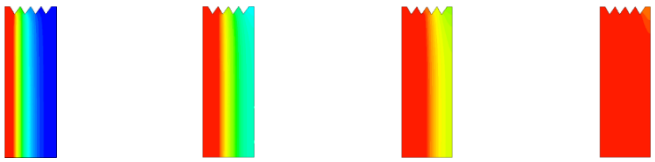			
R-60°				

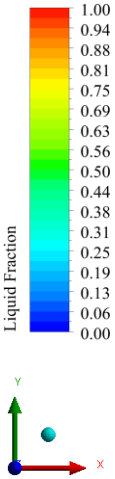

Figure 6 illustrates the influence of MF and the IA of triangular fins on the melting process. Considering the melting time provides important insights in terms of evaluating the thermal response time of the system and determining the heat transfer efficiency. The results indicate that the inclusion of MF significantly reduced the melting time by approximately 87.5 times. This reduction can be attributed to the enhanced effective thermal conductivity of the system, which facilitates better heat conduction and increases thermal diffusion within the domain. Furthermore, MF was found to alter the system's characteristics. As shown in Figure 6(a), the shortest melting time in the absence of MF was observed for the 120° configuration.

However, with the addition of MF, this behavior shifted, and the R-60° configuration achieved the fastest melting time, as depicted in Figure 6(b). The reason for this difference, as mentioned before, is that MF exhibits homogeneous behavior due to heat being transferred via conduction. The accelerated melting of PCM in the presence of MF can be explained by the significant improvement in effective thermal conductivity. This enhancement, combined with the synergistic effects of heat conduction and heat convection, resulted in a faster melting rate of the PCM when MF was included in the system.

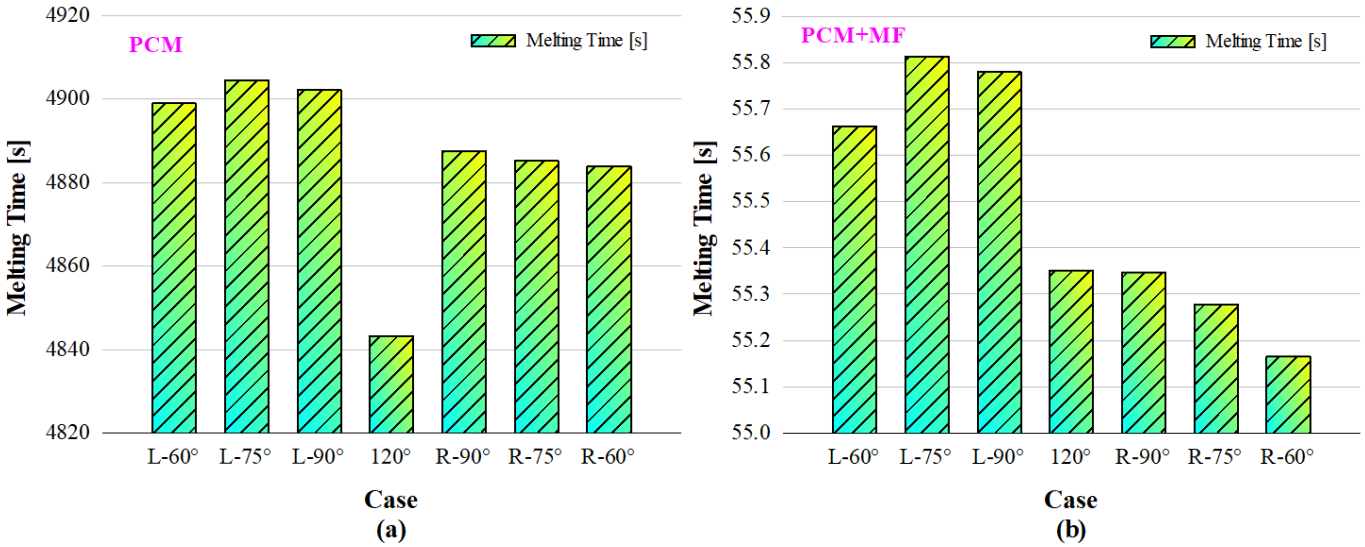

Figure 6. Comparison of melting time considering different IAs for; (a) without MF and (b) with MF.

Figure 7 depicts the temporal average temperature variation in the LHTES systems including different triangle fin configurations. In these applications, evaluating PCM temperature change is crucial for defining the system's phase change process and understanding the heat transfer dynamics. It is clearly mentioned that temperature changes show a sudden increase in the early stage of melting (pre-sensible) for both without MF and with MF cases due in that time heat dominantly progresses with conduction. After the starting of the melting, the latent heat process is observed and temperature variations show a more horizontal tendency.

The results, also, indicate that the highest final temperature was achieved in the R-60° configuration for both cases. The final temperature was recorded as 334.91K without MF and 334.75K with MF.

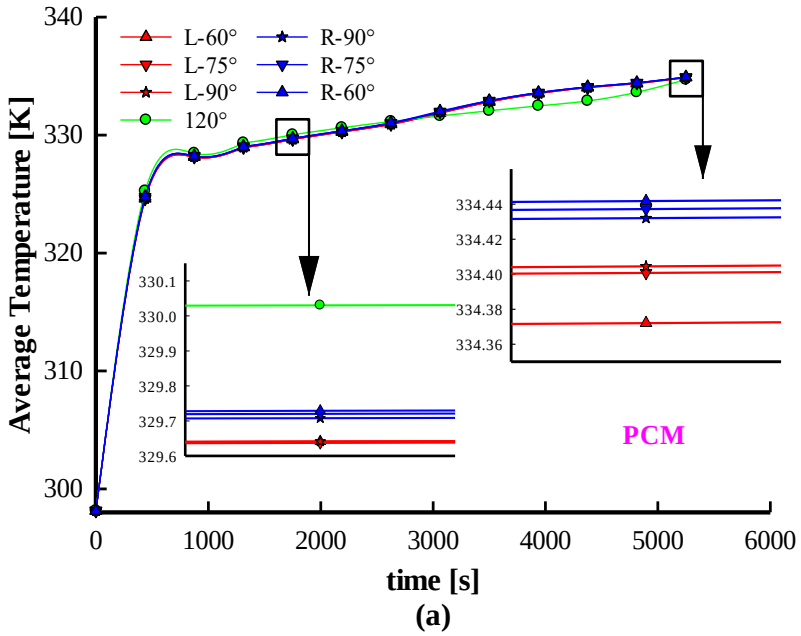

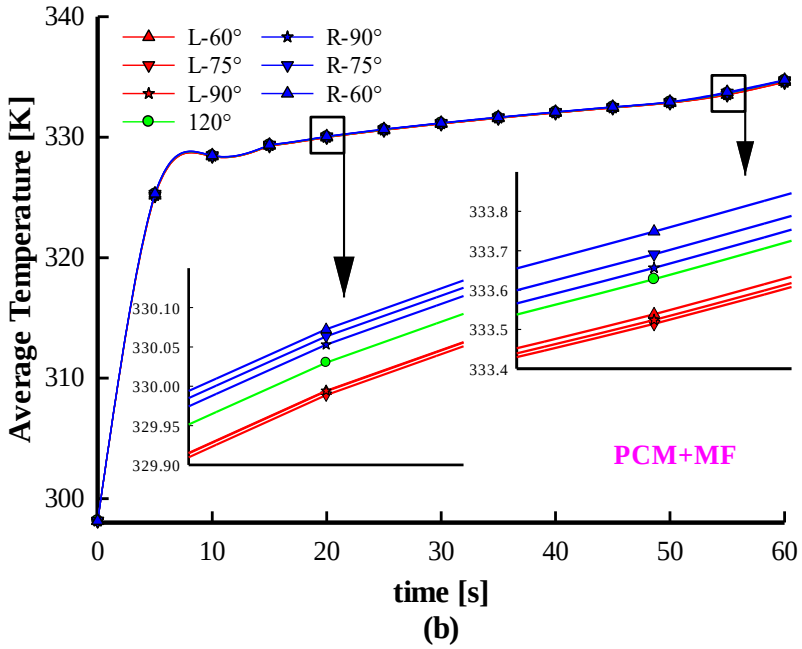

Figure 7. Average temperature versus time considering different IAs for; (a) without MF and (b) with MF.

The velocity profiles of the cases with different triangular IAs, without and with MF, on the horizontal (0, 15 mm; 10 mm, 15 mm) and vertical (5 mm, 0; 5 mm, 30 mm) lines are presented in Figure 8 for fully melted condition. In these applications, discussion of the speed changes in the system is an important indicator of heat transfer effectiveness and understanding the phase change process. When examining the horizontal velocity profiles, it is evident that the MF exerts a significant influence on the velocity distribution within the rectangular cavity. The velocity is observed to be highest in regions adjacent to the lateral walls, with elevated velocity values near the heated wall. This phenomenon is attributed to the thermal gradient established by the heated wall, which induces density variations in the PCM due to thermal expansion. The less dense, heated material ascends along the heated wall, while the denser, cooler material descends along the opposing walls, generating natural convection currents. These convective flows are most pronounced near the walls, where the thermal gradients are steepest, resulting in higher velocities in these regions. Conversely, the velocity values in the central region of the cavity consistently decrease under all conditions. The central region behaves as a "stagnation zone" where the interaction of upward and downward convective currents from opposing walls reduces the net velocity. Notably, under without MF conditions, the lowest velocity profiles occur in the L-60° configuration, whereas under MF influence, the R-60° configuration yields the highest velocity levels.

The effect of MF is also distinctly observable in the vertical velocity profiles. In without MF scenarios, velocity increases near the bottom of the cavity, whereas MF presence leads to a more uniform velocity distribution. Under MF conditions, regions of heightened velocity are shifted toward the upper wall, coinciding with the locations of fins. Furthermore, while the L-60° configuration exhibits the lowest velocity without MF cases, L-90° demonstrates the highest velocity distribution under MF conditions. These findings underscore the critical role of MF in modulating flow dynamics and enhancing velocity distribution within the cavity.

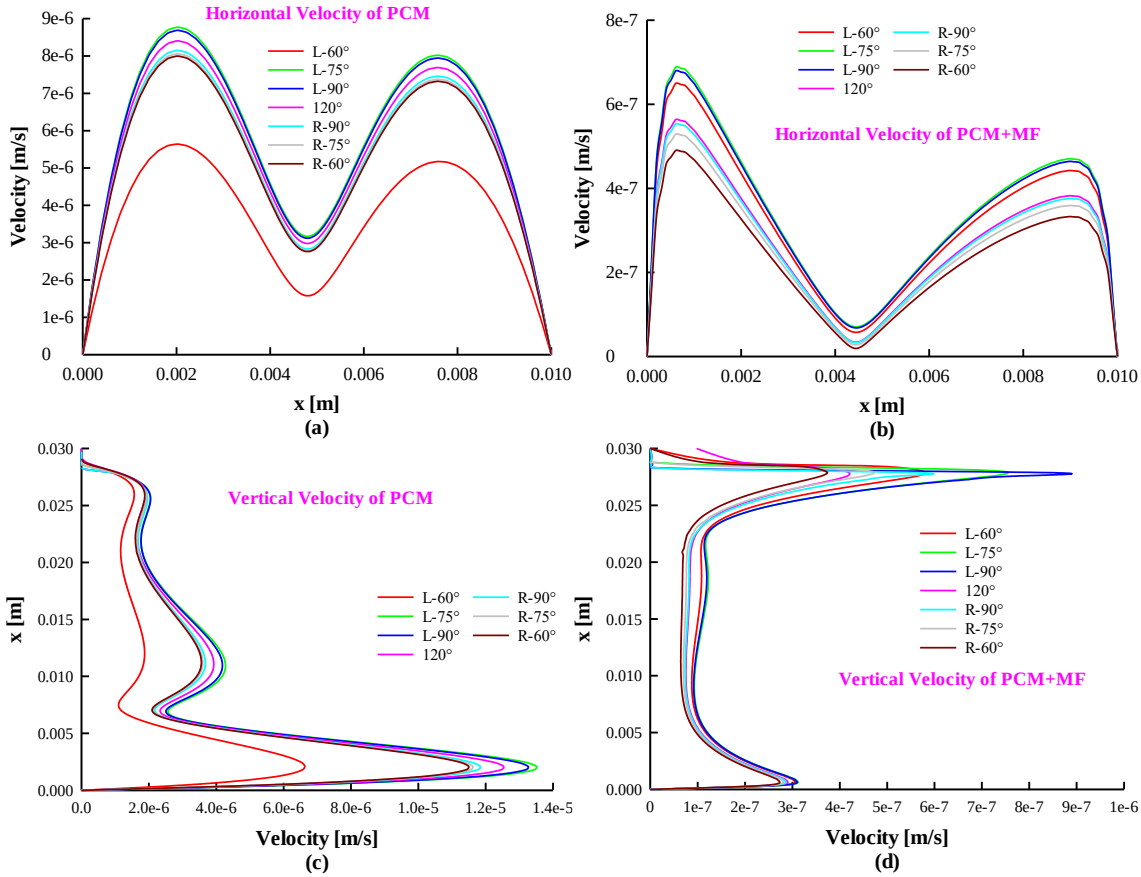

Figure 8. Velocity profile for; (a) without MF horizontal direction, (b) with MF horizontal direction, (c) without MF vertical direction, and (d) with MF vertical direction.

Demonstrating the results of ΔH changes in PCM applications provides a pioneering approach to determining energy storage capacity, design, and material selection. Figure 9 compares the ΔH performance of systems with and without MF over time for unit horizontal length. The results show that the ΔH trends are similar across both scenarios. Moreover, the energy storage process in systems with MF is more uniform, mirroring the homogeneity observed in liquid fraction and average temperature distributions. When the results are examined, it is calculated that the highest amount of stored energy is partially realized for the MF and without MF states of R-60°. In addition, when the without MF state and the MF state are compared for the full melting state, it is determined that the without MF state stores 5.69% more energy. The factor that causes this situation is that there is an aluminum material in the volume that should be PCM in the MF state, and this factor reduces the amount of energy stored in the MF state.

Another important situation determined is that the state containing MF stores higher energy from the beginning of the melting until the average temperature of the PCM reaches T_L=332K. At this point, the important issue and the decision which is within the user/system requirements is whether the full melting time or the total amount of stored energy is important. It is recommended that researchers optimize the porosity structures of the MFs to be used in LHTESs regarding this issue.

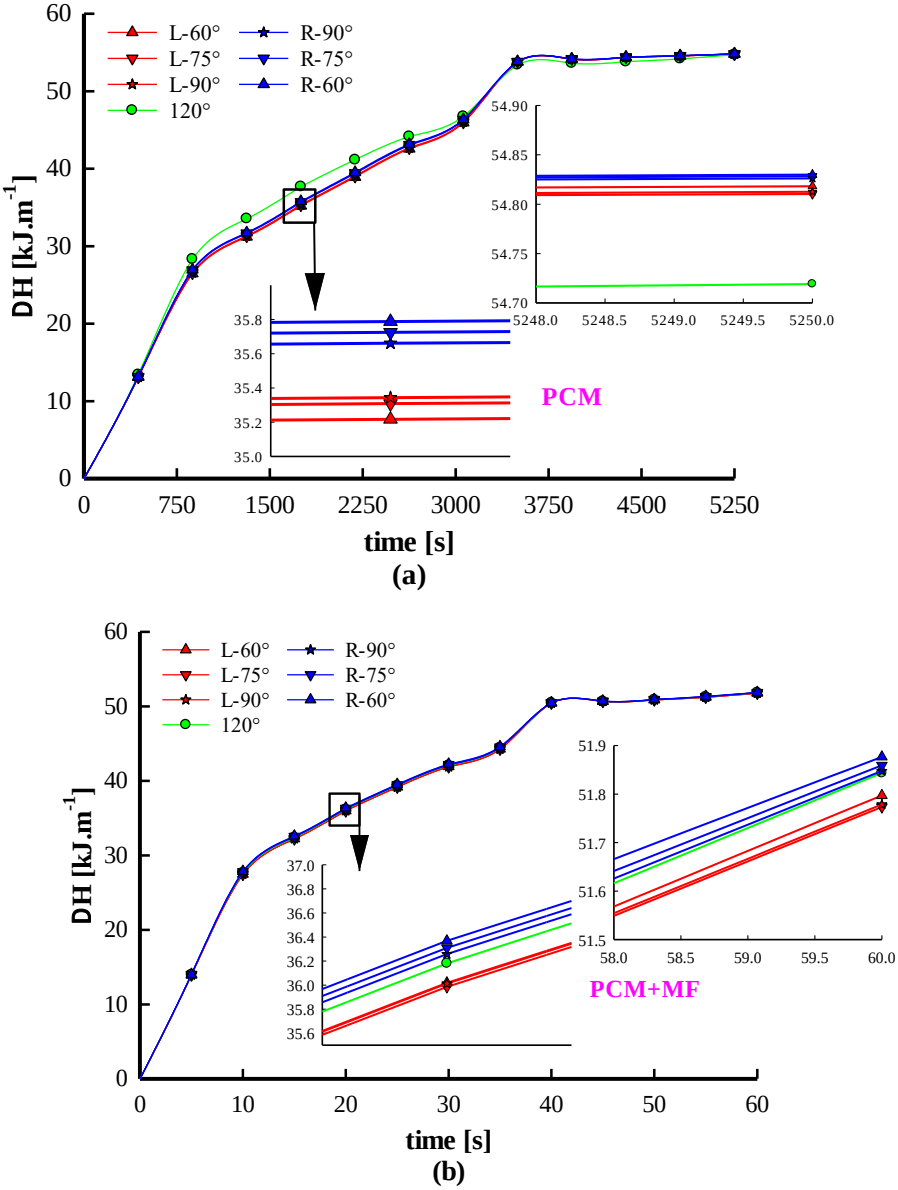

Figure 9. Energy storage versus time considering different IAs for; (a) without MF and (b) with MF.

IV. CONCLUSION

This study evaluates the performance of LHTES systems by investigating the effects of different IA triangular fins and MF. Key parameters such as liquid fraction, melting time, average temperature, and energy storage have been analyzed. The systems incorporate RT58 (Rubitherm) as PCM and aluminum MF with ε=0.9 and ω=20 PPI. In all simulations, the Brinkman-Darcy-Forchheimer model and enthalpy-porosity method were employed to solve the governing equations and model the melting process under the LTE hypothesis. The main findings are summarized as follows:

- *Reduction in Melting Time:* MF reduced the melting time by approximately 87.5 times due to the enhanced effective thermal conductivity, allowing heat to be conducted more efficiently within the cavity and increasing thermal diffusion.
- *Homogeneity of Liquid Fraction:* The PCM embedded within MF displayed a more uniform liquid fraction compared to the PCM without MF.

- *Melting Time Trends:* The shortest melting time occurred at 120° for systems without MF, while cases with MF experienced the earliest melting at R-60°, driven by the combined effects of enhanced heat conduction and convection.
- *Energy Storage:* Systems without MF exhibited higher energy storage than those with MF at the rate of 5.69% for R-60° since the volume occupied by the MF material is filled by the PCM which can store energy. The maximum amount of the stored energy is realized as 54.83 kJ.m-1.
- *Homogeneous Energy Storage:* Similar to the trends in liquid fraction and average temperature, the energy storage process in MF cases was more uniform, with the highest energy storage recorded as 51.87 kJ.m-1 at R-60°.
- *Possible studies:* In the next studies, the effects of different fin structures, the effects of different MF characteristics, the effects of nanoparticle use, the effects of magnetic field application and ultrasonic vibration application, and the cases including the combination of these applications can be addressed. Studies on the melting process and energy storage performance of LHTES can be conducted and also the solidification process of the system can be investigated.

CONFLICTS OF INTEREST

They reported that there was no conflict of interest between the authors and their respective institutions.

RESEARCH AND PUBLICATION ETHICS

In the studies carried out within the scope of this article, the rules of research and publication ethics were followed.

REFERENCES

[1] S. Tan and X. Zhang, "Progress of research on phase change energy storage materials in their thermal conductivity," *J. Energy Storage*, vol. 61, p. 106772, 2023, doi: https://doi.org/10.1016/j.est.2023.106772.

[2] B. K. Choure, T. Alam, and R. Kumar, "A review on heat transfer enhancement techniques for PCM based thermal energy storage system," *J. Energy Storage*, vol. 72, p. 108161, Nov. 2023, doi: 10.1016/J.EST.2023.108161.

[3] G. Liu *et al.*, "Experimental and numerical studies on melting/solidification of PCM in a horizontal tank filled with graded metal foam," *Sol. Energy Mater. Sol. Cells*, vol. 250, p. 112092, 2023, doi: https://doi.org/10.1016/j.solmat.2022.112092.

[4] S. Liu, H. Wang, Q. Ying, and L. Guo, "Numerical study on the combined application of multiple phase change materials and gradient metal foam in thermal energy storage device," *Appl. Therm. Eng.*, vol. 257, p. 124267, 2024, doi: https://doi.org/10.1016/j.applthermaleng.2024.124267.

[5] M. Xing, Z. Zhang, D. Jing, and H. Chen, "Enhanced solidification/melting heat transfer process by multiple copper metal foam for ice thermal energy storage," *J. Energy Storage*, vol. 79, p. 110207, 2024, doi: https://doi.org/10.1016/j.est.2023.110207.

[6] C. Yang *et al.*, "Analysis of charging performance of thermal energy storage system with graded metal foam structure and active flip method," *J. Energy Storage*, vol. 99, p. 113254, 2024, doi: https://doi.org/10.1016/j.est.2024.113254.

[7] S. Shen, H. Zhou, Y. Du, Y. Huo, and Z. Rao, "Investigation on latent heat energy storage using phase change material enhanced by gradient-porosity metal foam," *Appl. Therm. Eng.*, vol. 236, p. 121760, 2024, doi: https://doi.org/10.1016/j.applthermaleng.2023.121760.

[8] A. Alasmari *et al.*, "A shell-tube latent heat thermal energy storage: Influence of metal foam inserts in both shell and tube sides," *Int. Commun. Heat Mass Transf.*, vol. 159, p. 107992, 2024, doi: https://doi.org/10.1016/j.icheatmasstransfer.2024.107992.

[9] M. Bouzidi, M. Sheremet, K. Shank, S. Tiari, and M. Ghalambaz, "Charging and discharging heat transfer improvement of shell-tube storage utilizing a partial layer of anisotropic metal foam," *J. Energy Storage*, vol. 79, p. 109948, 2024, doi: https://doi.org/10.1016/j.est.2023.109948.

[10] W. Ahmed, A. Hussain, H. Shahid, I. Ali, and H. M. Ali, "Experimental Study on Heat Storage Properties Comparison of Paraffin/Metal Foams Phase Change Material Composites," *J. Therm. Sci.*, vol. 33, no. 2, pp. 469–478, 2024, doi: 10.1007/s11630-023-1828-5.

[11] A. Nassar *et al.*, "Enhancing the thermal transfer properties of phase change material for thermal energy storage by impregnating hybrid nanoparticles within copper foams," *Results Eng.*, vol. 21, p. 101885, 2024, doi: https://doi.org/10.1016/j.rineng.2024.101885.

[12] J. Liu, Y. Xiao, and C. Nie, "Pore-scale study of melting characteristic of phase change material embedded with novel open-celled metal foam," *Int. J. Heat Mass Transf.*, vol. 228, p. 125634, 2024, doi:

https://doi.org/10.1016/j.ijheatmasstransfer.2024.125634.
[13] Z. Du, X. Huang, Y. Li, X. Yang, and M.-J. Li, "Design and study of metal foam parameters on whole melting-solidification cycle in phase change heat storage system," *Int. J. Heat Fluid Flow*, vol. 106, p. 109299, 2024, doi: https://doi.org/10.1016/j.ijheatfluidflow.2024.109299.
[14] A. Moaveni, M. Siavashi, and S. Mousavi, "Passive and hybrid battery thermal management system by cooling flow control, employing nano-PCM, fins, and metal foam," *Energy*, vol. 288, p. 129809, 2024, doi: https://doi.org/10.1016/j.energy.2023.129809.
[15] C. Yang *et al.*, "Melting performance analysis of finned metal foam thermal energy storage tube under steady rotation," *Int. J. Heat Mass Transf.*, vol. 226, p. 125458, 2024, doi: https://doi.org/10.1016/j.ijheatmasstransfer.2024.125458.
[16] Y. Lu *et al.*, "Melting enhancement in a shell-and-tube latent heat storage unit with staggered fin-foam synergistic configuration," *J. Energy Storage*, vol. 82, p. 110505, 2024, doi: https://doi.org/10.1016/j.est.2024.110505.
[17] S. Rahmanian, Rahmanian-Koushkaki, M. H., Moein-Jahromi, and M. Setareh, "Numerical thermal performance assessment of phase change process in a PCM/foam-fins enclosure under various thermal conditions," *Energy Sources, Part A Recover. Util. Environ. Eff.*, vol. 46, pp. 2360–2376, 2024, doi: https://doi.org/10.1080/15567036.2024.2304642.
[18] P. M. Z. Hasan, N. H. Abu-Hamdeh, O. K. Nusier, A. M. Hussin, and H. A. Saad, "Energy storage analysis during melting in presence of metallic fins via numerical method," *J. Energy Storage*, vol. 66, p. 107454, 2023, doi: https://doi.org/10.1016/j.est.2023.107454.
[19] S. Zhang, L. Pu, L. Xu, and M. Dai, "Study on dominant heat transfer mechanism in vertical smooth/finned-tube thermal energy storage during charging process," *Appl. Therm. Eng.*, vol. 204, p. 117935, 2022, doi: https://doi.org/10.1016/j.applthermaleng.2021.117935.
[20] A. S, A. Sharma, and H. B. Kothadia, "Performance analysis of PCM melting in a fin-assisted thermal energy storage system – A numerical study," *Int. Commun. Heat Mass Transf.*, vol. 144, p. 106747, 2023, doi: https://doi.org/10.1016/j.icheatmasstransfer.2023.106747.
[21] M. K. Fahad, N. F. Ifraj, M. R. Haque, N. M. Chowdhury, and Fatema-Tuj-Zohora, "Numerical investigation on consecutive charging and discharging of PCM with Modified longitudinal fins in shell and tube thermal energy storage," *Results Eng.*, vol. 24, p. 103577, 2024, doi: https://doi.org/10.1016/j.rineng.2024.103577.
[22] S. D. Farahani, A. D. Farahani, A. J. Mamoei, and W.-M. Yan, "Enhancement of phase change material melting using nanoparticles and magnetic field in the thermal energy storage system with strip fins," *J. Energy Storage*, vol. 57, p. 106282, 2023, doi: https://doi.org/10.1016/j.est.2022.106282.
[23] C. Ao, S. Yan, L. Zhao, and Y. Wu, "Assessment on the effect of longitudinal fins upon melting process in a latent heat thermal energy storage unit," *J. Energy Storage*, vol. 59, p. 106408, 2023, doi: https://doi.org/10.1016/j.est.2022.106408.
[24] Z. Du, X. Huang, Y. Li, G. Liu, X. Yang, and B. Sundén, "Experimental Study on Melting and Solidification Cycle of a Hybrid Pin Fin/Metal Foam Energy Storage Tank," *ASME J. Heat Mass Transf.*, vol. 146, no. 8, p. 82401, 2024, doi: 10.1115/1.4065349.
[25] X. Huang, Z. Du, Y. Li, X. Yang, and M.-J. Li, "Numerical and optimization study on heat storage and release process of novel fin-metal foam composite structures under periodic heat source," *Int. J. Heat Fluid Flow*, vol. 108, p. 109445, 2024, doi: https://doi.org/10.1016/j.ijheatfluidflow.2024.109445.
[26] K. Zeng *et al.*, "Comprehensive enhancement of melting-solidifying process in latent heat storage based on eccentric fin-foam combination," *Energy*, vol. 313, p. 133693, 2024, doi: https://doi.org/10.1016/j.energy.2024.133693.
[27] A. NematpourKeshteli, M. Iasiello, G. Langella, and N. Bianco, "Increasing melting and solidification performances of a phase change material-based flat plate solar collector equipped with metal foams, nanoparticles, and wavy wall-Y-shaped surface," *Energy Convers. Manag.*, vol. 291, p. 117268, 2023, doi: https://doi.org/10.1016/j.enconman.2023.117268.
[28] I. Afaynou, H. Faraji, K. Choukairy, A. Arshad, and M. Arıcı, "Heat transfer enhancement of phase-change materials (PCMs) based thermal management systems for electronic components: A review of recent advances," *Int. Commun. Heat Mass Transf.*, vol. 143, p. 106690, Apr. 2023, doi: 10.1016/J.ICHEATMASSTRANSFER.2023.106690.
[29] T. Chen *et al.*, "Investigation and optimal design of partially encapsulated metal foam in a latent heat storage unit for buildings," *J. Energy Storage*, vol. 84, p. 110979, 2024, doi: https://doi.org/10.1016/j.est.2024.110979.
[30] B. Buonomo, H. Celik, D. Ercole, O. Manca, and M. Mobedi, "Numerical study on latent thermal energy storage systems with aluminum foam in local thermal equilibrium," *Appl. Therm. Eng.*, vol. 159, p. 113980, 2019, doi: https://doi.org/10.1016/j.applthermaleng.2019.113980.
[31] W. Lin, G. Xie, J. Yuan, and B. Sundén, "Comparison and Analysis of Heat Transfer in Aluminum Foam Using Local Thermal Equilibrium or Nonequilibrium Model," *Heat Transf. Eng.*, vol. 37, no. 3–4, pp. 314–322, Mar. 2016, doi: 10.1080/01457632.2015.1052682.
[32] A. D. Canonsburg, "ANSYS Fluent User ' s Guide," no. August. ANSYS, Inc., 2018.
[33] B. Buonomo, M. R. Golia, O. Manca, S. Nardini, and R. E. Plomitallo, "External heat losses effect on shell and tube latent heat thermal energy storages partially filled with metal foam," *J. Energy Storage*, vol. 85, p. 111096, Apr. 2024,

doi: 10.1016/J.EST.2024.111096.
[34] C. Nie, J. Liu, and S. Deng, "Effect of geometry modification on the thermal response of composite metal foam/phase change material for thermal energy storage," *Int. J. Heat Mass Transf.*, vol. 165, p. 120652, Feb. 2021, doi: 10.1016/J.IJHEATMASSTRANSFER.2020.120652.
[35] S. Huang, J. Lu, and Y. Li, "Numerical study on the influence of inclination angle on the melting behaviour of metal foam-PCM latent heat storage units," *Energy*, vol. 239, p. 122489, Jan. 2022, doi: 10.1016/J.ENERGY.2021.122489.
[36] F. Oflaz, "Evaluation of the thermo-hydraulic behavior of water-based graphene and Al2O3 hybrid nanofluids in a circular tube through CFD simulations," *J. Therm. Anal. Calorim.*, 2025, doi: 10.1007/s10973-025-13993-4.
[37] M. H. Zolfagharnasab, M. Salimi, and C. Aghanajafi, "Application of non-pressure-based coupled procedures for the solution of heat and mass transfer for the incompressible fluid flow phenomenon," *Int. J. Heat Mass Transf.*, vol. 181, p. 121851, 2021, doi: https://doi.org/10.1016/j.ijheatmasstransfer.2021.121851.
[38] T. Saeed, "Influence of the number of holes and two types of PCM in brick on the heat flux passing through the wall of a building on a sunny day in Medina, Saudi Arabia," *J. Build. Eng.*, vol. 50, p. 104215, 2022, doi: https://doi.org/10.1016/j.jobe.2022.104215.
[39] S. Patankar, *Numerical heat transfer and fluid flow*. CRC press, 2018.
[40] H. K. Versteeg, *An introduction to computational fluid dynamics the finite volume method, 2/E*. Pearson Education India, 2007.
[41] C. Z. Ji, Z. Qin, Z. H. Low, S. Dubey, F. H. Choo, and F. Duan, "Transient numerical study on enhancement of phase change material thermal storage with angled parallel fins," 2017.
[42] Ansys Inc., "Ansys Fluent User Guide," 2019. https://www.afs.enea.it/project/neptunius/docs/fluent/html/th/node352.htm

JOURNAL OF SCIENCE, TECHNOLOGY AND ENGINEERING RESEARCH
Bilim, Teknoloji ve Mühendislik Araştırmaları Dergisi
ISSN (Online) 2717-8404
Available *online* at https://dergipark.org.tr/en/pub/jster

RESEARCH ARTICLE

Human Instance Segmentation Based on Omega- Shape Using Deep Learning

* Huma Sheraz, [1] Zuhaib Ahmed Khan, and [2] Muhammad Awais[3]

*National University of Modern Languages NUML, Faculty of Computing, Software Engineering Department, Islamabad, Pakistan
Huma.sheraz@numl.edu.pk https://orcid.org/0009-0002-8562-7947
[1]Mirpur University of Science and Technology, Mirpur Azad Kashmir, Pakistan
engr.zohaib01@gamil.com https://orcid.org/0009-0007-4849-1303
[2] Capital University of Science and technology, Faculty of Computing, Software Engineering Department, Islamabad, Pakistan
Mawaiskhan1808@gmail.com https://orcid.org/0009-0006-3101-524X

Citation:
Sheraz, H., Khan, Z.A., Awais, M. (2025). Human Instance Segmentation Based on Omega- Shape Using Deep Learning, *Journal of Science Technology and Engineering Research*, 6(1): 31-41. DOI: 10.53525/jster.1469697

HIGHLIGHTS

- *Advances detection accuracy*
- *Collaborative insights from varied*
- *Refinement of human detection methods*
- *Pivotal for future advancements*

Article Info

Received **:** April 17, 2024
Accepted **:** February 7, 2025

DOI:
10.53525/jster.1469697

***Corresponding Author:**

Muhammad Awais
mawaiskhan1808@gmail.com
Phone: +92 3418977385

ABSTRACT

Human detection and segmentation in an unconstrained environment is a very important and difficult task, having many important applications including tracking human beings, pedestrian detection, head count etc. Human detection in a single object environment is quite easy, but the problem becomes quite cumbersome in a crowded and cluttered environment. Most of the existing algorithms work on the detection and segmentation of the whole person in a scene. However, the performance of such algorithms degrades in case of occlusion and cluttered environment. To increase the performance in such an environment a technique is available that detects a distinct part of the human body which is "omega shape" instead of the full human body. However, the detection of bounding box also includes background pixels which limit the performance of the high-end applications such as tracking. Therefore, the objective of this research is to accurately segment the omega shape, so that the high-end applications have no background clutter in the human appearance model. We have trained and evaluated Mask R-CNN and YOLO+UNET and got a trade-off between accuracy and computation cost. The testing accuracy of Mask R- CNN and YOLO+UNET is 92.6% and 88.4%, while the computation cost is 6fps and 29fps, respectively.

Keywords: *Deep Learning, Omega-shape, Pedestrian-Detection, Instance Segmentation*

I. INTRODUCTION

This document In this century, with the increase in computational power, the concept of Computer Vision(CV) has caught attention in the field of security, agriculture, and segmentation. Segmentation is the process of segregation of a digital image into multiple homogeneous parts. The objective of segmentation is: 1) to change the illustration of an image for ease of analysis and 2) recognition. Mask R-CNN [1] is the state-of-art segmentation algorithm but it lags in term of execution time due to its multi stage network. So, this paper pays attention on computation time and proposes a method for real time human segmentation. It is very important because it has been widely used in security, head-count, pedestrian detection, driver-less cars, and human tracking.

Human tracking is the process of following and locating person in the video. With the recent advancements in the field of object detection, most researchers performed multiple human tracking by the process of tracking-by-detection. Tracking by detection has two steps. The first step is human detection and the second step is instance matching. Human detection in a scene is quite a cumbersome task even today due to the variation in pose and occlusion of the human body. To tackle pose variation and occlusion, we propose a detection technique in which only omega shape (it includes head, torso, and arms) is detected. The bounding box (with white boundary) in fig 1 shows the omega-shaped of the human body. This helps vastly as variations in pose and occlusion caused by a crowded environment does change and occupy the omega shape in most cases. Another major challenge in human detection is back- ground clutter which results in problematic instance matching. Therefore, this paper also focuses on instance segmentation of the human body using omega-shape features.

The contributions of our work can be summarized as:

- Implementation of an automated system for the instance segmentation of human.
- To tackle the pose and occlusion problem.
- To speed up the instance segmentation process.

Figure 1. Omega-shape

II. LITERATURE REVIEW

Human Detection is of vital importance in many fields. These fields include pedestrian detection, tracking, head count etc. Pedestrian detection is gaining wide popularity in applications like driverless technologies. Whereas, tracking is equally important in the problems like security. In complex environment where a large population and high occlusion is present, human detection becomes a harder job. A substantial amount of research in human detection and segmentation has been done in recent times. The researchers have opted three kinds of methods to achieve

aforementioned task which are, rule-based method, traditional machine learning based methods and deep learning-based methods.

There are several methods for solving computer vision problems by manipulating the images based on a specific rule without applying any learning. Such methods are known as rule-based methods. Among those, there are only few techniques which work in real conditions for a long period of time [2]. Methods for human detections demonstrated in [3], [4]. Works on a supposition that a person will appear in an occlusion free environment for a time period, giving enough time for a model of the pedestrian to be built up while it is isolated from occlusion. The techniques presented in [3], [4], [5], [6] are the examples of algorithms which fail in real time environments which are unconstrained. The reason behind the failure of algorithms in a real environment is that they rely on color intensity. The techniques described in [7], [8], [9], [10] employ periodic features attained from a time-based set of frames for human detection. In [11] a system with high reliability is introduced which integrate various nods such as face, shape pattern and color to detect humans. Nevertheless, face detection can detect only pedestrian facing towards camera and color is very sensitive to illumination changes. The problems with Rule based algorithms are quite evident in the above-mentioned algorithms i.e. they require presence of constrained environment, and their performance suffer in the unconstrained environment.

In the last decade, some quite efficient traditional machine learning based algorithms for pedestrian detection are created. There are different detectors which employ different sets of features and classification methods. A popular technique which involves linear SVM classifier in combination with HOG features is presented by Dalal and Triggs [12]. This algorithm, when applied on the INRIA dataset provided superior performance. Following the technique produced by the researchers in [12], many researchers have modified the HOG based method by introducing extra features which include color information [13], LBP [14], second order statistical measures [15], [16], and many other methods to boost the performance in comparison with the original detector. However, it also increased the computational cost of detectors. A cascade-based detector ACF proposed by Dollar et al [17], uses histograms of augmented orientation with color information treated as differentiating structures and subsequently, they used Adaboost based classifiers for the classification purpose [13]. To enhance the speed of detection, ACF estimates features among various scales to avoid unnecessary computations. This detector was a breakthrough in the field of human detection. Authors in [15] proposed a SPF detector which is a significant enhancement on ACF detector. This algorithm improves the collections of features used by ACF to take in an LBP variant, full 360-degree orientations of calculated gradients and spatial gradients of second order. Authors in [18], [19] demonstrated a detailed analysis of the individual features used by various known detectors such as HOG and ACF and their influence on the final detection performance. In all of the above algorithms full humans are detected. These algorithms provide degraded performance in environment with high occlusion and clutter. This problem can be rectified by using Omega-Shape features. The method proposed by researchers in [20] used such features by deploying Viola-Jones Adaboost classifier along with local HOG features. The most important factor while implementing the traditional machine learning algorithms mentioned is the selection of features. These selected features, if not selected properly will make the model over-fit during the process of learning, which results in loss of performance during test time.

Convolutional neural networks (CNN) algorithms for human detection are propelled by the accomplishment of CNNs in various detection-based tasks. Some of the works of incorporating CNNs in pedestrian detection are [21], [22], [23], [24], [25], [6]. They mostly employed R-CNN [26] which is a two- stage network for detection. Furthermore, in these techniques, rule- based detectors such as ICF [27] and its improvements [28], [29], [30] were deployed for region proposals, followed by a CNN to classify the pre-planned areas once more. CNN presented in [31] employed convolutional sparse coding to train the model basic parameters, and then fine-tuned on the Caltech dataset. Very Fast proposed in [32] created a CNN based cascade, that uses a small CNN to filter candidates before passing through to a deep CNN. F-DNN explained in [33] employed a fused multiple CNNs and soft cascade mechanism in the stage two cascade. The Faster R-CNN presented in [34] has become a standard model for detection of general object, but it underperforms when applied to pedestrian detection problem without any modification. This is because of the background clutter and low resolution of object [35]. Higher performance can be achieved when boosted decision forest was deployed on top of convolution feature maps [35], [36], [37]. There are still other approaches which still show top performance. These algorithms involve customized CNNs derived from Faster R-CNN architectures [38], [39]. Researchers in [40] revealed that after proper modification, a simple Faster R-CNN model can be similar to the state of the art in terms of performance. The problem with previously mentioned techniques is that they detect a whole human body, which reduces the performance of the CNNs significantly in an environment with partially occluded human

bodies. The human bodies have a distinct omega shape which can be detected even in occluded environment. The authors in [41] used a deep Omega-shape feature learning and multi-paths detection to make the detector more efficient to human pose variations and scale changes. The problem with omega shape human detection is that the presence of background pixels in the bounding box reduces the performance of high-level application of human tracking, because appearance model has background pixels in addition to foreground human pixels. The algorithm presented in [42], rectifies the problem created by background pixels in an environment where whole human shape is segmented. Our proposed methodology performs instance segmentation of human, based on omega shape features using deep learning techniques to overcome the above-mentioned problems.

Present-day deep learning methods, such fully convolutional neural networks, address several important remote sensing issues, including the identification and segmentation of artificial land objects on extremely high-resolution hyperspectral map sceneries and the utilization of non-visible bandwidths. The three components of the solution are the creation of the dataset, the neural network, and the neural network fine-tuning. The initial section of the solution proposes a semi-automated approach for quickly creating datasets with contemporary technologies while maintaining the benefits of remote sensing imaging, such extremely high resolution and the ability to use a range of visual and thermal hyperspectral imagery bandwidths. The current research offers a method for solving the problem of remote sensing images segmentation using deep fully convolutional neural networks, which can be used to demonstrate the use of a dataset. The binary classifier for a dataset is constructed based on Mask RCNN, and the best deep learning architectures for instance segmentation are taken into consideration and examined. Using several configurations and optimizers, the final neural network architecture with the new classifier is adjusted to maximize the benefits of the created hyperspectral remote sensing dataset [47].

Design of a revolutionary iterative deep reinforcement learning agent that can simultaneously learn to distinguish between several items. Using a graph coloring approach, we have built our reward function for the trainable agent to favor grouping pixels that belong to the same item. We show that instance segmentation of several objects may be accomplished rapidly with the suggested technique without requiring extensive post-processing [48].

Introduce Poly-YOLO, an improved version of Yolo that incorporates instance segmentation for improved efficiency. Expanding upon the concepts of YOLOv3, Poly-YOLO eliminates two of its drawbacks: an excessive number of rewritten labels and an ineffective anchor distribution. By employing stair step up sampling and a hyper column approach to aggregate data from a light SE-Darknet-53 backbone and provide a single scale output with high resolution, Poly-YOLO lessens the problems. While only 60% of Poly-YOLO's parameters are trainable, it increases the mean average accuracy by a relative 40% when compared to YOLOv3. Additionally, we propose Poly-YOLO lite, which has a lower output resolution and fewer parameters. While it is twice as quick and three times smaller as YOLOv3, it has the same accuracy and is therefore appropriate for embedded systems. Lastly, Poly-YOLO uses bounding polygons to do instance segmentation. The network is taught to identify polygons on a polar grid that are size-independent. Poly-YOLO generates polygons with different numbers of vertices since each polygon's vertices are predicted together with their confidence [49].

Introduce SeqFormer, a tool for segmenting video instances. SeqFormer constructs instance connections among video frames by utilizing the vision transformer idea. However, we note that, in order to capture a temporal sequence of instances in a video, a stand-alone instance query is sufficient; however, attention methods must be applied to each frame separately. In order to accomplish this, SeqFormer finds an instance in every frame and then combines temporal data to learn a strong representation of a video-level instance. This representation is then utilized to dynamically anticipate the mask sequences on every frame. Without post-processing or branch tracking, instance tracking occurs organically. Without bells and whistles, SeqFormer achieves 47.4 AP on YouTube-VIS with a ResNet-50 backbone and 49.0 AP with a ResNet-101 backbone. This accomplishment greatly outperforms the prior state-of-the-art by 4.6 and 4.4, respectively. Furthermore, when combined with the recently suggested Swin transformer, SeqFormer attains a significantly higher AP of 59.3 [50].

Introduce OSFormer, the first one-stage disguised instance segmentation (CIS) transformer framework. OSFormer is built around two main concepts. Firstly, by incorporating location-guided queries and blend-convolution feed-forward network, we construct a location-sensing transformer (LST) to retrieve the location label and instance-aware parameters. Secondly, we create a coarse-to-fine fusion (CFF) to combine various context data from the CNN backbone

and LST encoder. By combining these two elements, OSFormer may effectively combine local characteristics and distant context dependencies to forecast instances that are concealed. Our OSFormer exhibits high convergence efficiency and reaches 41% AP when compared to two-stage frameworks without requiring a large amount of training data [51].

Figure 1. Images from PASCAL-part Dataset [43]

III. METHOD

As discussed, our work is about the instance segmentation of omega-shape using deep learning techniques. We used the Pascal-part dataset, which is publicly available [43]. We trained Mask R-CNN and YOLO+UNET and used pre-trained weights for the training of Mask R-CNN and YOLO, while we trained UNET from scratch. Dataset and proposed model architecture are discussed in the following sections.

A. Dataset

As discussed in the previous section that pascal-part is a publicly accessible dataset. This dataset is a set of additional annotations for PASCAL VOC 2010 [44]. The dataset consists of 20 classes i.e. human, vehicle, boat, etc. We have used 3,503 images of human class in which 2,452 (70%) are used for training and 1051 (30%) for validation and testing. Fig 2 shows some sample images of human class.

Mask R-CNN

Mask R-CNN [1] is the extended version of Faster R-CNN for pixel-level instance segmentation. Instance segmentation is the task to locate each object in the class, predict its class and provide a binary mask for each object in that class. At the high level, the Mask RCNN consists of feature pyramid network and backbone layer, followed by region proposal network which generates positive region (object) and bounding box refinement.

We selected the Mask R-CNN as our model [1]. The model choice is based on the following consideration; first Mask R-CNN can achieve advanced results on a range of object detection tasks. One such example is that Mask R-CNN has beaten the top models in the most recent COCO competition for object detection. Secondly, the Mask R-CNN algorithm is a quite simple and bendable technique system for object detection and object instance segmentation. In addition, the model can be easily implemented with pre-trained weights in Keras and TensorFlow library, and the model can be accessed on GitHub, which happens to be an open-source repository.

The current work implemented the same network architecture as defined in the Mask R- CNN paper. Mask R-CNN model is based on two base phases. The first phase scans the image input, and then provides an output called proposal (also called the region of interest (ROI)), which is the area where object is likely to be present. The second phase classifies the region and generates the bounding box and masks. At high level, the Mask RCNN consists of Feature Pyramid Network plus Backbone, followed by region proposal network which generates positive region (object) and bounding box refinement. A mask basically is, a CNN based network which, out of ROI, digs out the positive regions and then generates a mask for them. The various components of our Mask R-CNN algorithm design and their functionality are discussed below.

The Convolutional Res-Net backbone and FPN: Residual Network (Res-Net) [51] was introduced initially as CNN to perform the image classification task but it became a popular choice for other deep learning tasks. Residual networks enable us to efficiently train deep neural network simply by introducing skip connections, in which weights coming from previous layers, are copied into more deep layers. In our model, ResNet101 (a variant of Res-Net) serves as a

basic CNN network of our network which serves as a feature extractor in this specific application. The initial layers detect the parameters like edges, corners etc. (low-level features) and the deep layers detect higher features. This backbone layer processes the images at the input, and outputs them into the feature map in the last layer. He et al. used RestNet101 in combination with Feature pyramid network (FPN) to serve as a backbone layer.

Region proposal Network (RPN): The next RPN layer in Mask RCNN architecture scans the input images in "sliding window" method and is an easy-to- go neural network. It finds the area which contains the object. RPN scans over the extracted feature of backbone and it increases the performance and efficiency of the network. The RPN scan over the region is called anchors. There are more than 200k anchors for an image. The RPN generates two classes from each anchor. These two classes are; bounding box refinement and anchor class. Anchor class has one of two classes i.e. foregrounds (object) and background. While bounding box ensures to fit the object better by refining the anchor perfectly.

Non-max Suppression (NMS): Using RPN, the algorithm picks the top anchor in which the objects are probable to exist and then approximate their location in close proximity. If there are multiple overlapped anchors, the one with the highest foreground score will be chosen and this process is known as NMS. After this, the final Region of interest (ROI) is passed to the next stage.

ROIAlign: It is used to extracts ROIs on feature maps and then scale them to the same size. The ROIAlign is designed to fix the misalignment problem, which is that the scaled size output is not the same position as the original ROI's position.

Classifier and Regressor: This layer generates two outputs for each ROI i.e. it's class and bounding box around each class.

Segmentation mask: Another CNN based network, the Segmentation Mask branch takes the fixed-size feature map and generates the mask for them. During the inference mode, the predicted mask is resized to the ROI bounding box of original size and provides the final mask for each object.

B. Yolo+UNET

Mask R-CNN is quite accurate, but it lags in terms of execution speed. To increase the execution speed of segmentation, we proposed a new technique which is a combination of YOLO [45] and UNET [46]. YOLO+UNET can be divided into 3 phases. Yolov3 which is the first part, suggests the region of interest (ROI), and regresses for the classes and confidence scores. In the thesis, a modified YOLOv3 is implemented, which also output the feature maps from different layers of the residual blocks. The second part is ROIAlign that takes different YOLO bounding box outputs and feature maps as inputs and generates the fixed-size ROI feature maps. UNET is the last part, which transforms the ROI inputs to the mask outputs. The whole model architecture is shown in the below fig 3. The detailed architecture is discussed below.s

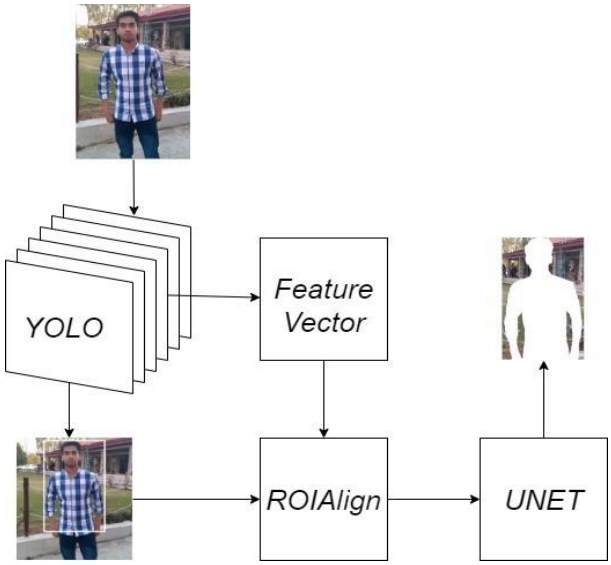

Figure 3. YOLO+UNET Model Pipeline

Yolo: You only look once (YOLO) is an end-to-end network for object detection. Many cutting- edge technology is generated by the 3rd generation of YOLO, which is YOLOv3. YOLO splits the image to SxS block, and then it is the responsibility of each block to detect those targets whose center points fall within the grid. To eliminate the duplicate bounding boxes Non-Maximum Suppression is used after detection. The network includes residual block-based backbone, feature pyramid network like network head for multi-scale prediction, batch normalization, anchor boxes prediction etc. These details of the network are discussed below.

	Type	Filter	Size	Output
	Convolutional	32	3x3	256x256
	Convolutional	64	3x3/2	128x128
1x	Convolutional	32	1x1	
	Convolutional	64	3x3	
	Residual			128x128
	Convolutional	128	3x3/2	64x64
2x	Convolutional	64	1x1	
	Convolutional	128	3x3	
	Residual			64x64
	Convolutional	256	3x3/2	32x32
8x	Convolutional	128	1x1	
	Convolutional	256	3x3	
	Residual			32x32
	Convolutional	512	3x3/2	16x16
8x	Convolutional	256	1x1	
	Convolutional	512	3x3	
	Residual			16x16
	Convolutional	1024	3x3/2	8x8
4x	Convolutional	512	1x1	
	Convolutional	1024	3x3	
	Residual			8x8

Figure 4. Darknet53 Architecture

Darknet53:Darknet53 is an efficient backbone for performing feature extraction. It is a very deep backbone that contains 53 convolutional layers. It conveys many advanced structures including: (a) Residual blocks which add shortcut layers to make the network easier to train; (b) Inception structure, that contains 3x3, 1x1 convolutional kernel, which keeps the respective field and decreases the computation cost; (c) Batch normalization layer makes the learning of layers in the network more independent of each other. With the high efficiency of the Darknet53, it is selected as the feature extractor for both YOLOv3 head and for later segmentation done by us. Darknet53 architecture is shown in fig 3.

Feature Vector Formation for Segmentation: As shown in fig 5, We extract the feature vector of different size from the backbone layers, which are 5,10,26 and we name them V1, V2, and V3 accordingly. When the layer goes more in-depth, the size of the feature map reduces to half of the previous layer. Then we up-sample V2, V3 and do the feature concatenation with their previous feature map. Because in networks when we go deeper into the layers we lose lower-level information about boundaries, edges, and contours. So, to recover this information we take features from lower layers and concatenate them with higher.

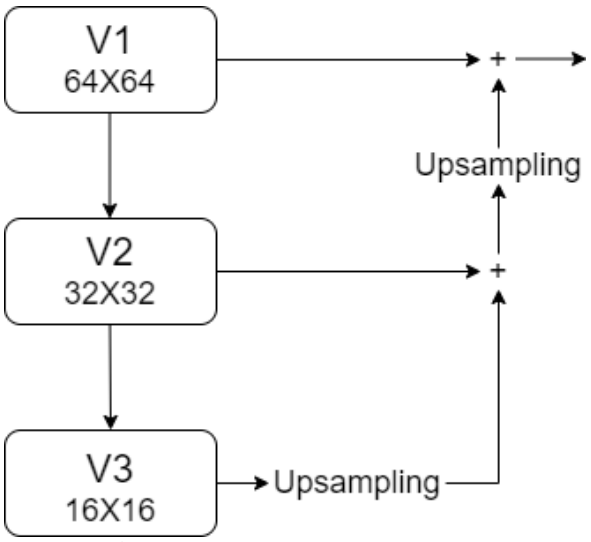

Figure 5. Feature Vector Extraction

UNET: UNET is an object segmentation algorithm that does not depend on a region proposal network. It was designed by Olaf Ronneberger et al. [46] for biomedical image segmentation. It is an encoder-decoder framework for object segmentation.

UNET architecture comprises of two phases. First phase is the construction phase (encoder) that captures the context in the image. It is just a stack of CNN and max-pooling layers. The second phase is the expanding path (decoder). It is used for exact localization using transposed convolutional. UNET is an end- to-end a fully convolutional network as it just comprises of convolutional layers. We reduced layers of UNET from 26 to 14 because the input size is 28x28 and at sixth layer feature vector size reduces to 7X7. In our modified YOLO+UNET model, YOLO detects the bounding boxes of each instance than ROI-Align crops these instances from the feature vector. UNET takes each cropped instance one by one as input and gives the segmented output.

IV. RESULT

Our models are trained on a NVIDIA GeForce RTX2060. We have implemented Mask R- CNN with FPN plus Res-Net-101 as a backbone network, and YOLO with backbone Darknet53 with modified UNET for segmentation. We used open-source deep learning framework Keras and TensorFlow for model implementatoin. For the training of Mask R- CNN and YOLO, we used the model transfer learning method.

A. Model Performance

We compare Mask R-CNN with YOLO+UNET. We trained both the models using the same dataset and the same GPU. Speed and accuracy performance are discussed in the following sections.

Speed Performance: First, we performed a speed comparison between Mask R-CNN and YOLO+UNET. Since the YOLO is a single-stage network that's why we achieved real-time 29 frames per second (FPS) segmentation with YOLO+UNET, and it is 4.8 times faster than Mask R-CNN segmentation.

Accuracy Performance: Secondly, we conducted an experiment regarding accuracy. Mask R-CNN achieved 92.6% and YOLO+UNET achieved 88.4%. Experimental results show that YOLO+UNET's accuracy is less with the difference of 4.2% which is not a big difference compared to the speed improvement of YOLO+UNET over the Mask R-CNN.

In terms of speed as it is 4.8 times (48%) faster than Mask R-CNN. We also compute the segmentation accuracy of both models by dropping the instances from the ground truth which are not detected by the models. The segmentation accuracy. The difference is only 1.2% which shows that YOLO+UNET and Mask R-CNN has almost the same segmentation performance. Some sample qualitative results of Mask R-CNN and YOLO+UNET.

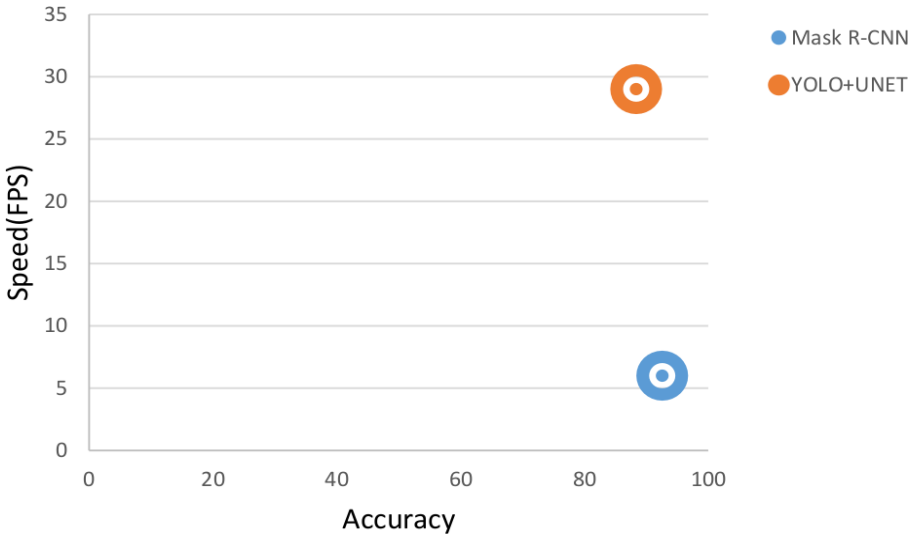

Figure 6. Speed Accuracy Tradeoff

Detection Performance: We also conducted experiments regarding the detection of omega-shape. The detection performance for both the models. The accuracy of YOLO is 3.09% less than Mask R-CNN which affect the segmentation accuracy of YOLO from these experiments we concluded that Mask R-CNN and YOLO+UNET has almost the same segmentation accuracy.

This hybrid technique to human instance segmentation has never been employed before, combining state-of-the-art models Mask R-CNN, YOLO, and UNET. The precision of Mask R-CNN in region-based segmentation, YOLO's real-time detection capabilities, and UNET's potent feature extraction for fine-grained segmentation are all tapped into in this innovative combination to provide a more reliable and precise framework. The study illustrates its advancements by contrasting its findings with those of earlier research. In particular, it compares performance to current human instance segmentation models in terms of speed (FPS), accuracy (mIoU, Precision, Recall, F1-score), and detection (AP, AP@50, AP@75). By incorporating Omega-Shape features into segmentation, the limitations of conventional methods are addressed and boundary refinement and object discrimination are further improved. This study outperforms traditional strategies by introducing a novel fusion mechanism that maximizes both detection and segmentation accuracy.

V. CONCLUSION

In this research, we trained Mask R-CNN and YOLO+UNET for the instance segmentation of human using omega shape feature on Pascal part dataset. For the training of Mask R- CNN and YOLO, we used pre-trained weights (from COCO Dataset), but not for UNET because we changed its layers. Furthermore, we evaluated our models over accuracy and speed performance. During the experiment, we concluded that Mask R-CNN gives results with an accuracy of 92.6% which is good enough and shows its reliability. However, the speed of Mask R-CNN is 6FPs, so to enhance the speed we developed another model namely YOLO+UNET. Experimental results showed that YOLO+UNET is 4.8 times faster than Mask R-CNN while, its accuracy is 88.4%, which is 4.2% less than that of Mask R- CNN. This is a very good trade off in terms of speed over accuracy. Therefore, a segmentation model for real-time usage is developed which can be used for real-time high- end applications like tracking.

CONFLICTS OF INTEREST

All the authors of this paper declare that there is no conflict of interests regarding the publication of this manuscript.

RESEARCH AND PUBLICATION ETHICS

The research conceptualization and methodology were done by Huma Sheraz. The technical and theoretical framework was prepared by Zuhaib Ahmed Khan. The technical review and improvement were performed by Muhammad Awais.

ACKNOWLEDGMENT

Thankfully, we are aware of our parent's affection for us. Last but not least, we would like to thank our family and friends whose prayers made it possible for us to finish this project.

REFERENCES

[1]. M. Harville, "Stereo person tracking with adaptive plan-view templates of height and occupancy statistics," Image and Vision Computing, vol. 22, no. 2, pp. 127–142, 2004.

[2]. A. Senior et al., "Tracking people with probabilistic appearance mod- els," in ECCV workshop on Performance Evaluation of Tracking and Surveillance Systems. Citeseer, 2002, pp. 48–55.

[3]. A. Elgammal and L. S. Davis, "Probabilistic framework for segmenting people under occlusion," in Proceedings Eighth IEEE International Conference on Computer Vision. ICCV 2001, vol. 2. IEEE, 2001, pp. 145–152.

[4]. W. Hu, M. Hu, X. Zhou, T. Tan, J. Lou, and S. Maybank, "Principal axis-based correspondence between multiple cameras for people track- ing," IEEE Transactions on Pattern Analysis and Machine Intelligence, vol. 28, no. 4, pp. 663–671, 2006.

[5]. J. Rittscher, P. H. Tu, and N. Krahnstoever, "Simultaneous estimation of segmentation and shape," in 2005 IEEE Computer Society Conference on Computer Vision and Pattern Recognition (CVPR'05), vol. 2. IEEE, 2005, pp. 486–493.

[6]. C.-J. Pai, H.-R. Tyan, Y.-M. Liang, H.-Y. M. Liao, and S.-W. Chen, "Pedestrian detection and tracking at crossroads," Pattern Recognition, vol. 37, no. 5, pp. 1025–1034, 2004.

[7]. B. Heisele and C. Woehler, "Motion-based recognition of pedestrians," in Proceedings. Fourteenth International Conference on Pattern Recog- nition (Cat. No. 98EX170), vol. 2. IEEE, 1998, pp. 1325–1330.

[8]. R. Cutler and L. S. Davis, "Robust real-time periodic motion detection, analysis, and applications," IEEE Transactions on Pattern Analysis and Machine Intelligence, vol. 22, no. 8, pp. 781–796, 2000.

[9]. S. A. Niyogi, E. H. Adelson et al., "Analyzing and recognizing walking figures in xyt," in CVPR, vol. 94, 1994, pp. 469–474.

[10]. ——, "Analyzing and recognizing walking figures in xyt," in CVPR, vol. 94, 1994, pp. 469–474.

[11]. N. Dalal and B. Triggs, "Histograms of oriented gradients for human detection," in 2005 IEEE computer society conference on computer vision and pattern recognition (CVPR'05), vol. 1. IEEE, 2005, pp. 886–893.

[12]. P. Dolla´r, R. Appel, S. Belongie, and P. Perona, "Fast feature pyramids for object detection," IEEE transactions on pattern analysis and machine intelligence, vol. 36, no. 8, pp. 1532–1545, 2014.

[13]. X. Wang, T. X. Han, and S. Yan, "An hog-lbp human detector with partial occlusion handling," in 2009 IEEE 12th international conference on computer vision. IEEE, 2009, pp. 32–39.

[14]. S. Paisitkriangkrai, C. Shen, and A. van den Hengel, "Pedestrian detec- tion with spatially pooled features and structured ensemble learning," IEEE transactions on pattern analysis and machine intelligence, vol. 38, no. 6, pp. 1243–1257, 2015.

[15]. T. Watanabe and S. Ito, "Two co-occurrence histogram features using gradient orientations and local binary patterns for pedestrian detection," in 2013 2nd IAPR Asian Conference on Pattern Recognition. IEEE, 2013, pp. 415–419.

[16]. S. Maji, A. C. Berg, and J. Malik, "Classification using intersection kernel support vector machines is efficient," in 2008 IEEE conference on computer vision and pattern recognition. IEEE, 2008, pp. 1–8.

[17]. R. Benenson, M. Mathias, T. Tuytelaars, and L. Van Gool, "Seeking the strongest rigid detector," in Proceedings of the IEEE Conference on Computer Vision and Pattern Recognition, 2013, pp. 3666–3673.

[18]. S. Zhang, R. Benenson, B. Schiele et al., "Filtered channel features for pedestrian detection." in CVPR, vol. 1, no. 2, 2015, p. 4.

[19]. M. Li, Z. Zhang, K. Huang, and T. Tan, "Rapid and robust human detection and tracking based on omega-shape features," in 2009 16th IEEE International Conference on Image Processing (ICIP). IEEE, 2009, pp. 2545–2548.

[20]. J. Hosang, M. Omran, R. Benenson, and B. Schiele, "Taking a deeper look at pedestrians," in Proceedings of the IEEE conference on computer vision and pattern recognition, 2015, pp. 4073–4082.

[21]. S. Zhang, R. Benenson, M. Omran, J. Hosang, and B. Schiele, "How far are we from solving pedestrian detection?" in Proceedings of the iEEE conference on computer vision and pattern recognition, 2016, pp. 1259–1267.

[22]. Y. Tian, P. Luo, X. Wang, and X. Tang, "Deep learning strong parts for pedestrian detection," in Proceedings of the IEEE international conference on computer vision, 2015, pp. 1904–1912.

[23]. ——, "Pedestrian detection aided by deep learning semantic tasks," in Proceedings of the IEEE conference on computer vision and pattern recognition, 2015, pp. 5079–5087.

[24]. D. Ribeiro, J. C. Nascimento, A. Bernardino, and G. Carneiro, "Im- proving the performance of pedestrian detectors using convolutional learning," Pattern Recognition, vol. 61, pp. 641–649, 2017.

[25]. R. Girshick, J. Donahue, T. Darrell, and J. Malik, "Rich feature hierarchies for accurate object detection and semantic segmentation," in Proceedings of the IEEE conference on computer vision and pattern recognition, 2014, pp. 580–587.

[26]. P. Dolla´r, Z. Tu, P. Perona, and S. Belongie, "Integral channel features," 2009.

[27]. P. Dolla´r, R. Appel, S. Belongie, and P. Perona, "Fast feature pyramids for object detection," IEEE transactions on pattern analysis and machine intelligence, vol. 36, no. 8, pp. 1532–1545, 2014.

[28]. W. Nam, P. Dolla´r, and J. H. Han, "Local decorrelation for improved pedestrian detection," Advances in neural information processing sys- tems, vol. 27, pp. 424–432, 2014.

[29]. R. Benenson, M. Mathias, T. Tuytelaars, and L. Van Gool, "Seeking the strongest rigid detector," in Proceedings of the IEEE Conference on Computer Vision and Pattern Recognition, 2013, pp. 3666–3673.
[30]. P. Sermanet, K. Kavukcuoglu, S. Chintala, and Y. LeCun, "Pedestrian detection with unsupervised multi-stage feature learning," in Proceed- ings of the IEEE conference on computer vision and pattern recognition, 2013, pp. 3626–3633.
[31]. A. Angelova, A. Krizhevsky, V. Vanhoucke, A. Ogale, and D. Ferguson, "Real-time pedestrian detection with deep network cascades," 2015.
[32]. X. Du, M. El-Khamy, J. Lee, and L. Davis, "Fused dnn: A deep neural network fusion approach to fast and robust pedestrian detection," in 2017 IEEE winter conference on applications of computer vision (WACV). IEEE, 2017, pp. 953–961.
[33]. S. Ren, K. He, R. Girshick, and J. Sun, "Faster r-cnn: Towards real-time object detection with region proposal networks," IEEE transactions on pattern analysis and machine intelligence, vol. 39, no. 6, pp. 1137–1149, 2016.
[34]. L. Zhang, L. Lin, X. Liang, and K. He, "Is faster r-cnn doing well for pedestrian detection?" in European conference on computer vision. Springer, 2016, pp. 443–457.
[35]. Q. Hu, P. Wang, C. Shen, A. van den Hengel, and F. Porikli, "Pushing the limits of deep cnns for pedestrian detection," IEEE Transactions on Circuits and Systems for Video Technology, vol. 28, no. 6, pp. 1358– 1368, 2017.
[36]. Z. Cai, M. J. Saberian, and N. Vasconcelos, "Learning complexity-aware cascades for pedestrian detection," IEEE transactions on pattern analysis and machine intelligence, 2019.
[37]. J. Li, X. Liang, S. Shen, T. Xu, J. Feng, and S. Yan, "Scale-aware fast r- cnn for pedestrian detection," IEEE transactions on Multimedia, vol. 20, no. 4, pp. 985–996, 2017.
[38]. Z. Cai, Q. Fan, R. S. Feris, and N. Vasconcelos, "A unified multi-scale deep convolutional neural network for fast object detection," in European conference on computer vision. Springer, 2016, pp. 354–370.
[39]. S. Zhang, R. Benenson, and B. Schiele, "Citypersons: A diverse dataset for pedestrian detection," in Proceedings of the IEEE Conference on Computer Vision and Pattern Recognition, 2017, pp. 3213–3221.
[40]. Y. Xu, X. Zhou, P. Liu, and H. Xu, "Rapid pedestrian detection based on deep omega-shape features with partial occlusion handing," Neural Processing Letters, vol. 49, no. 3, pp. 923–937, 2019.
[41]. K. Chen, X. Song, X. Zhai, B. Zhang, B. Hou, and Y. Wang, "An integrated deep learning framework for occluded pedestrian tracking," IEEE Access, vol. 7, pp. 26 060–26 072, 2019.
[42]. Pascal voc 2010. [Online]. Available: http://roozbehm.info/pascal-parts/ pascal-parts.html
[43]. "Pascal voc 2010." [Online]. Available: http://host.robots.ox.ac.uk/ pascal/VOC/voc2010/index.html
[44]. J. Redmon and A. Farhadi, "Yolov3: An incremental improvement,"arXiv preprint arXiv:1804.02767, 2018.
[45]. O. Ronneberger, P. Fischer, and T. Brox, "U-net: Convolutional networks for biomedical image segmentation," in International Conference on Medical image computing and computer-assisted intervention. Springer, 2015, pp. 234–241.
[46]. Hnatushenko, V., & Zhernovyi, V. (2020, August). Method of improving instance segmentation for very high resolution remote sensing imagery using deep learning. In International Conference on Data Stream Mining and Processing (pp. 323-333). Cham: Springer International Publishing.
[47]. Anh, T. T., Nguyen-Tuan, K., Quan, T. M., & Jeong, W. K. (2020). Reinforced coloring for end-to-end instance segmentation. arXiv preprint arXiv:2005.07058.
[48]. Hurtik, P., Molek, V., Hula, J., Vajgl, M., Vlasanek, P., & Nejezchleba, T. (2022). Poly-YOLO: higher speed, more precise detection and instance segmentation for YOLOv3. Neural Computing and Applications, 34(10), 8275-8290.
[49]. Wu, J., Jiang, Y., Bai, S., Zhang, W., & Bai, X. (2022, October). Seqformer: Sequential transformer for video instance segmentation. In European Conference on Computer Vision (pp. 553-569). Cham: Springer Nature Switzerland.
[50]. Pei, J., Cheng, T., Fan, D. P., Tang, H., Chen, C., & Van Gool, L. (2022, October). Osformer: One-stage camouflaged instance segmentation with transformers. In European Conference on Computer Vision (pp. 19-37). Cham: Springer Nature Switzerland.

JOURNAL OF SCIENCE, TECHNOLOGY AND ENGINEERING RESEARCH
Bilim, Teknoloji ve Mühendislik Araştırmaları Dergisi
ISSN (Online) 2717-8404
Available *online* at https://dergipark.org.tr/en/pub/jster

RESEARCH ARTICLE

The Effect of Lighting and Curtain Automation on Energy Performance

[1]Orhun Celil Özen, *[2]Onur Akar, and [3]Nazmi Ekren

[1]Marmara University, Faculty of Technology, Electrical-Electronic Engineering Department, Istanbul, Türkiye
orhunozen@marun.edu.tr, Orcid.0009-0005-6007-708X
*[2]Marmara University, Vocational School of Technical Sciences, Electronics and Automation, Istanbul, Türkiye
onur.akar@marmara.edu.tr, Orcid.0000-0001-9695-886X
[3]Marmara University, Faculty of Technology, Electrical-Electronic Engineering Department, Istanbul, Türkiye
nazmiekren@marmara.edu.tr, Orcid.0000-0003-3530-9262

Citation:
Orhun C, O., Onur, A. Nazmi, E. (2025). *The Effect of Lighting and Curtain Automation on Energy Performance*, Journal of Science Technology and Engineering Research, 6(1): 42-53. DOI: 10.53525/jster.1613256

HIGHLIGHTS

- *Energy efficiency in office room lighting automation system has been examined annually.*
- *Different devices have been installed on the KNX system and programmed with ets6 and a test environment has been prepared*
- *It has been focused on how lighting automation affects work performance.*
- *A new approach has been introduced by using both natural and artificial light to keep work performance at a maximum level.*
- *Experiments have been carried out in 2 similar environments and energy performance has been evaluated.*

Article Info

Received **:** January 4, 2025
Accepted **:** March 29, 2025

DOI:
10.53525/jster.1613256

***Corresponding Author:**

Onur AKAR
onur.akar@marmara.edu.tr
Phone: +90 216 7774099

ABSTRACT

Energy efficiency in buildings has become a crucial factor in sustainable design and energy management. This study investigates the effects of lighting and curtain automation on energy performance, aiming to optimize energy consumption while maintaining indoor comfort. To achieve this, an automation system was developed to enhance the energy efficiency of lighting systems and prevent inefficient usage. The system, designed to address excessive or insufficient lighting in working and living areas, utilizes sensors to detect and automatically control light intensity through curtain blinds and brightness-adjustable lamps. This ensures that the environment remains at an optimal brightness level, reducing energy waste. The study employs an experimental approach, comparing two rooms—one equipped with the automation system and the other controlled manually—under similar environmental conditions. Light intensity and energy consumption were measured in both cases. In the automated room, light levels were adjusted dynamically using automated shutter movements and brightness-adjustable lamps, while in the non-automated room, manual control was used. The data comparison revealed that the automated system maintained a more stable light intensity and led to energy savings. Specifically, the manually controlled system consumed an average of 10.98 W, whereas the automation system consumed 10.09 W, resulting in an energy reduction of 0.9 W. Over six days, this led to a total energy saving of 130 W in a 20m² room. These findings highlight the potential of intelligent automation in reducing energy consumption and improving lighting efficiency in buildings. By integrating automation into lighting and shading systems, significant energy savings can be achieved, contributing to sustainability efforts and more efficient energy management.

Keywords: *Automation, KNX, Energy Efficiency, Sensor-based control, Smart Home System*

I. INTRODUCTION

The fact that energy use in buildings accounts for a significant proportion of global final energy consumption emphasizes that energy management is an essential part of long-term strategies focused on reducing energy consumption in buildings [1, 2]. The importance of improvements in this area becomes even more evident, especially in Europe, where buildings account for approximately 40% of energy consumption. With the revisions made within the framework of the European Green Deal, it reveals that the construction sector should play an important role in emission reduction by 2030. In order to achieve this target, buildings should be made more environmentally friendly and energy efficient [3].It has been determined that approximately 35% of electrical energy is used for lighting in buildings [4]. Many studies reveal that new buildings are not designed to reduce energy use. In most cases, building lighting systems cannot be managed efficiently. Even in some integrated lighting technology systems, energy efficiency cannot be achieved [5].According to the World Bank's 2008 building energy consumption report, building energy consumption is divided into various areas. According to this report, the lighting system of the building accounts for 31% of the total energy consumption, while other building components consume a total of 69%, including heating/cooling 36%, kitchen appliances 19% and entertainment 14% [6].The selection of the right light source, effective control systems and the use of energy efficient equipment provide significant energy savings. Multidimensional problems such as electrical lighting design and control of glare for visual comfort still persist [7]. Scientists have been working for many years to reduce this problem. Nowadays, people spend about 80% of their time inside buildings. Therefore, it is important to ensure lighting comfort [8-9]. In this context, there are many methods to increase energy efficiency today. However, in recent years, it is observed that building automation systems have become prominent in reducing electricity consumption. It is stated that the global market of automation systems is increasing and this trend continues [10]. Building automation systems not only optimize energy consumption, but also offer a number of advantages such as increasing comfort, ensuring safety an d reducing operating costs. In automation applications, heating and cooling systems can be managed more effectively thanks to smart thermostats. With motion sensors, lights can be switched off automatically and building security can be increased with security cameras. In addition, thanks to automation systems, functions such as indoor and outdoor lighting, curtain and shutter control become easily manageable. These features not only increase energy efficiency, but also significantly affect people's quality of life and work performance [11]. These values are calculated between 350-500 lx for most work areas [12]. Because the right lighting conditions are one of the important factors that determine people's mood, attention and productivity [13].

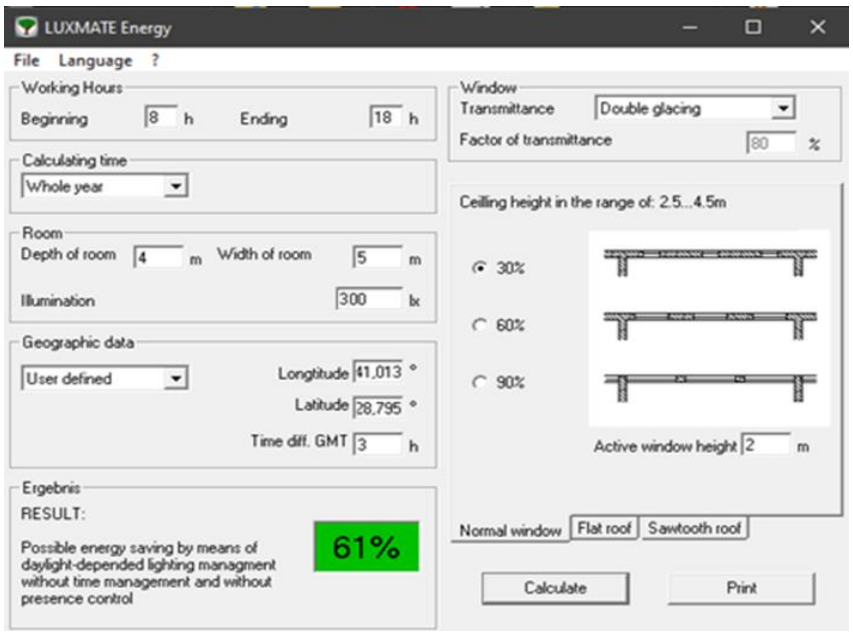

Figure. 1. Luxmate energy programmer calculation.

The designed automation system can automatically respond to changing lighting needs at different times and in different areas, taking these factors into account. It can adjust indoor lighting by adapting to changes in sunlight throughout the day or provide softer lighting in meeting rooms. This increases the comfort and productivity of employees while saving energy [14]. In the working model conducted with the luxmate energy programmer in Istanbul, it was calculated that possible energy savings can be up to 61%. As shown in Figure 1, the calculation is based on the assumption that employees work from 8:00 to 18:00 in a 4x5 m room with a window-to-wall ratio of 30%. Assuming a reception in this area, a total of 6000 lumens is required for this size of space. 8 lamps with approximately 700 lumens were determined to be suitable for this area. This arrangement brings the level to 300 lux, which is ideal for working when it is dark. When similar studies are analyzed, complex automation systems provide significant energy savings between 30% and 77% [15].As a result of automation studies in different sectors, it has been observed that automation systems used in the transport sector increase storage capacity by 27.27% [16]. Automated public transport lighting systems are more efficient than those in conventional rail systems, with around 35% traffic efficiency compared to under 20% for traditional systems [17]. In another study, consumption was drastically reduced from 400 W to 100 W with the PLC, indicating an energy saving potential of 75% with the proposed lighting control system [18]. A mixed automation study on a hotel showed that cascaded lighting control can reduce total annual energy consumption by 30-40%, [19].

In a similar study, artificial neural networks (ANN) and fuzzy logic were used to optimize the energy consumption of HVAC systems, achieving up to 20% savings. Additionally, genetic algorithms were employed to determine the optimal operating scenarios for smart building systems, improving efficiency. Machine learning models analyzed indoor temperature and user habits to develop automated energy management strategies[20]. In this study, unlike other studies, other efficiencies provided by air conditioning and automation were not taken into account, and the employee performance in a workplace was tried to be maximized by using the maximum natural light source. energy savings were calculated with experiments. This calculated energy saving was not calculated over 24 hours but was kept between real working hours. This working model shows that energy saving in the big picture can make a major contribution to global energy savings and climate change, considering the offices worldwide.

II. MANUSCRIPT PREPARATION

In the working model, 2 rooms with the same features on the same facade were selected and the lighting arrangement was made as in Figure 2. In the model without automation, a manual switch and 8 Ledwance brand 8W dimmable 700lm Dali compatible lamps were used. This system was operated with classical switching. In the 2nd room with similar features, KNX system was installed and curtain automation Dali dimming light intensity sensor and motion sensor were used. In the system, if there is no presence in the room, the lights are set to be switched off within 5 minutes if they are on. The data was recorded for 1 week. Since there are 2 rooms in the working environment, one room was used only to record lighting values and manual control was added later according to usage.For this working model, Legrand brand 002699 Dali controller 003507 KNX power supply and 002672 8 output actuator for curtain control were used. All devices were programmed and configured with KNX ETS6 software. Module connections for this model were used as shown in Figure 2.

A. KNX

KNX is a new European open standard approved by CENELEC in 2003 and adopted as an international standard in 2006. The KNX protocol is based on a decentralized architecture using negative logic to represent the bit structure. It uses four different media for data transmission: Twisted pair cable (TP), power line (PL), radio frequency (RF) and internet protocol (IP), the most widely used being KNX TP and KNX IP [20] . KNX is a globally recognized and used standard for building automation systems. This system has the ability to integrate various building automation applications such as energy management, lighting, security, heating, ventilation and air conditioning over a single network. The importance and advantages of KNX have been widely recognized in the building automation sector.
The KNX system enables devices manufactured by various manufacturers to work in harmony with each other. This

compatibility allows users to use products from different brands together. [21].KNX has a wide range of applications. This system can be used in both residential and commercial buildings. In residential buildings, it can fulfil various functions such as lighting control, integration of heating and cooling systems, security systems and energy management. In commercial buildings, KNX is widely used for energy monitoring, building management systems and integrated security solutions [22]. With its increasing integration with IoT in the future, KNX is expected to become even more widespread and continue to play a leading role in building automation [23].

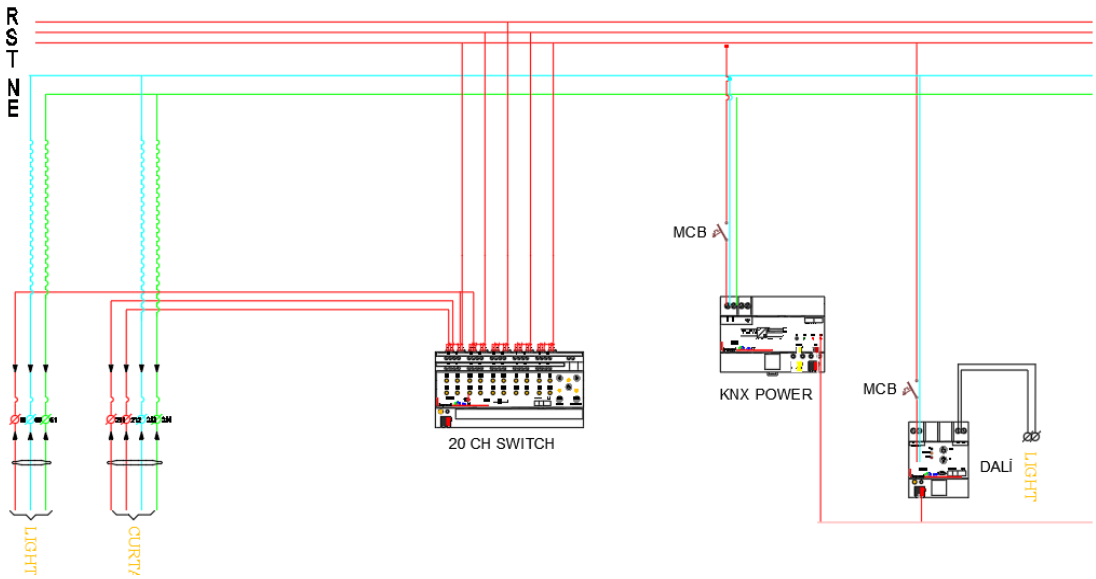

Figure. 2. KNX Modules electrical connection diagram.

B. DALI

DALI (Digital Addressable Lighting Interface) is a protocol that has become widespread especially in recent years for the management of modern lighting systems. This protocol is used to enable the communication of lighting luminaires and control devices and enables lighting systems to be more flexible, efficient and user-friendly [24]. DALI allows lighting luminaires to be controlled individually or in groups, so that different lighting scenarios can be created and energy savings can be achieved. Furthermore, the DALI protocol can be integrated with sensors and other automation devices, which increases automatic lighting control and user compliance. Used in both commercial and residential buildings, [25]. In this working model, the control of lighting was provided via DALI .In this study, while programming the selected DALI lighting power supplies, modules produced by Legrand brand and DALI programming software produced by EAE brand were used. With this software, DALI transformers were automatically addressed and then grouped from within the application and module to work together. Then, connection with the sensor was established via ETS and autonomous operation was ensured.

C. ETS6

ETS6 is a widely used building automation software in Europe, specially designed for the design, configuration and integration of KNX-based systems. This software covers all phases of building automation projects and allows users to easily manage complex systems. ETS6's features include advanced graphical interface, large device database, automatic device recognition and configuration, scenario generation and simulation, debugging and remote access. In addition, ETS6's integrated project management features enable large and complex projects to be organized and managed. ETS6 is considered as a reliable solution in the building automation industry and has become an industry standard for the design and management of KNX based systems. In this working model, all KNX devices were programmed with ETS6 and the system was monitored [26-29]. All KNX devices used in this study were programmed using ETS6 software. During the control processes, the Legrand 20-output module was configured

through ETS by combining outputs and setting them to curtain and blind mode. This setting synchronizes the outputs, preventing voltage from being sent to both the upward and downward wires of the curtain simultaneously, thus protecting the motors from damage. The sensor used in the study required only the input of the desired constant lux value through ETS, thanks to its internal algorithm. Based on this value, the sensor automatically generated the addresses needed to control the DALI drivers and, throughout the operation, sent percentage-based signals to the DALI power supply to maintain the lighting at the defined level. During the programming of the DALI control module, only the first group on the module was activated, and the emergency lighting was disabled. This ensured that in case of power outages or energy interruptions, the lamps would not enter a fault state and would retain their previous state. Additionally, the feedback feature of the DALI control module was enabled, allowing the system to monitor whether the DALI devices reached the desired levels and enabling intervention when necessary. This setup and programming approach not only improves energy efficiency but also optimizes the reliability of the system

D. WORKING ENVIRONMENT SETUP

A room was selected for the model as shown in Figure 3. This room is equipped with windows to allow external light to enter and there are 8 electric lamps for the interior lighting of the room. The room has the dimensions of a standard room with a width of 4 meters, a length of 5 meters and a height of 3 meters. The walls are dark in color and the ceiling of the room is covered with white plasterboard. The floor is carpeted and the furniture is minimal so that the number of reflective surfaces is minimized. During the research, other light sources in the room were switched off and the amount of light intensity was analyzed for 7 days. This environment provides a controllable environment to ensure accurate and repeatable measurement of light intensity.

Figure. 3. Furniture setup in my automated room.

E. LIGHTING SCHEME

A Modern lighting schemes improve the comfort and quality of life of users by illuminating spaces with a combination of energy efficiency, intelligent control systems and aesthetic design. These arrangements often include the use of lamps equipped with LED technology, resulting in lower energy consumption and longer life. Control devices such as motion sensors and timers integrated with intelligent building automation systems enable automated lighting management and automatic adjustment of appropriate lighting levels at different times and for different activities. Dynamic lighting scenarios can change the lighting level according to the needs of users and thus save

energy.
Therefore, modern lighting schemes improve the quality of life by providing more efficient, comfortable and aesthetic lighting of spaces. In this model, 8 piece 700 lumen lamps were used and placed as shown in Figure 4. The amount of light was monitored and controlled by Legrand 048922 sensor

F. AUTOMATION ALGORITHM

In the algorithm created for the working scenario, it is first checked whether there is a presence in the room. If a presence in the room cannot be detected for 5 minutes, the lighting is not switched on. If a presence is detected in the room, the illumination value is measured by the sensor. Since this room is used as a reception, this illumination value is tried to be kept at 300lux value. If the measured value is lower than 300, the curtain automation is activated first and the desired value is tried to be achieved by opening 1% each time. If the desired value is not achieved when the curtain is fully opened, the dimmable lamp is increased by 1% and the desired value is tried to be achieved. If the illumination value is higher than the desired value, the dimmable lamp is first reduced by 1% and the value is tried to be captured. This algorithm is summarized in Figure 5. in commercial, industrial and educational buildings, it reaches 40% of the total daily energy consumption. these algorithms try to prevent this .in different sources, 30% savings in energy consumption and 10% savings in operating costs can be achieved with lighting control.

Figure. 4. Lamp and sensor placement in the working area.

G. CALCULATION LUX VALUE

The lighting level of a room is usually measured in units of 'lux' (lux). Lux refers to the light intensity on a surface and 1 lux represents 1 lumen of light per square meter of surface. Lumens represent the total amount of light emitted by a light source. The lumen value emitted by each light source in the room should be known. This value is usually indicated on the lamps. For example, a conventional 60 watt light bulb emits approximately 800 lumens of light. The lighting used in this study emits 700 lumens of light. The calculation in Equation 1 is used to calculate lux.

$$Lux\ Val = \frac{Total\ Lumen}{Area} \quad (1)$$

When an area of 20m2 is examined for this study, approximately 280 lux value is found from this calculation.

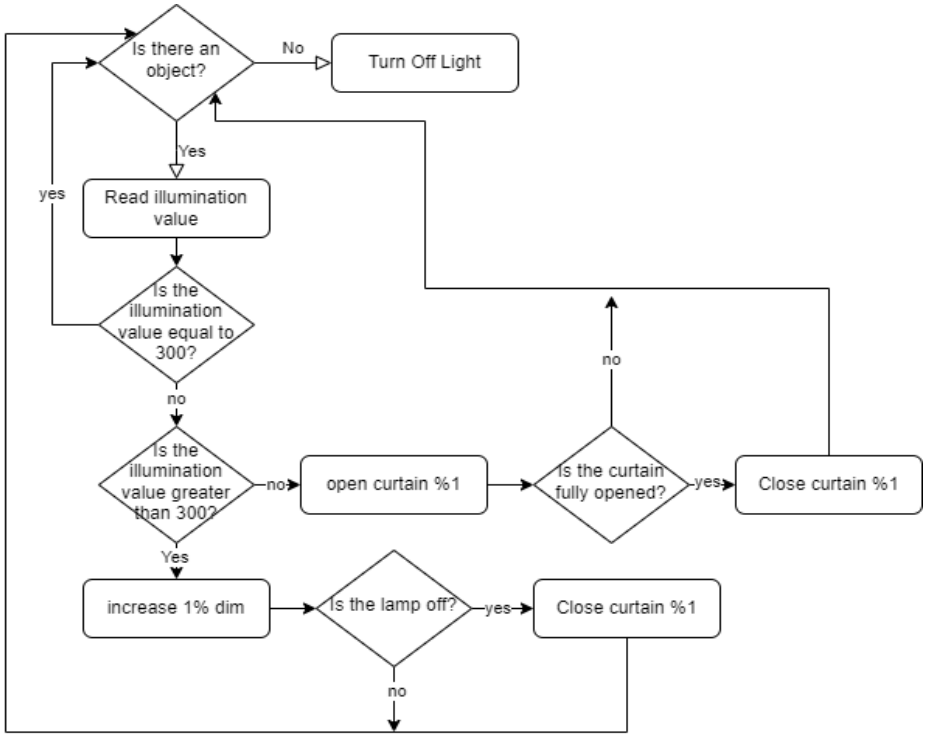

Figure. 5. Automation Algorithm.

H. MEASUREMENT DATA

In this test environment, the data were measured by sensors between 12 February 2024 and 17 February 2024 and recorded in 1 minute periods as shown in Figure 6. When the recorded 6-day data were analyzed, it was recorded that an average lux value above 300 was measured until 10:00 in the morning. At this point, the system is expected to reduce this value with curtain control. Later, when the sun started to approach the peak point, it was observed that the illumination value decreased to 300-400 lux band. The values, which continue in this way for a while, decrease as the sunset approaches and decrease to an average value of 100 lux. The illumination values were not in a certain distribution and followed a different behavior every day.

When the automation system works, it has managed to keep the illumination at a standard level of approximately 300 lux as shown in Figure 7, which increases the comfort of the employee by providing lighting suitable for the work he/she does all day long. When the energy consumed is examined, although the light was not manually switched on at some points, the automation tried to keep the lighting intensity constant by dimming a little, but when the 6-day working period was examined, the power graph in Figure 8 was revealed. When the total energy consumed during the total research (144 hour) process is divided by hours and examined, it is observed that in the system with manual switching on and off, an average of 10.98W power is consumed, while in the automation system, an average of 10.09W is consumed during the examination time, approximately 0.9W less energy is consumed for approximately 20m2 on average than the manual system. Unlike the simulation results, this situation was found to be approximately 8% more effective in real time test time. This difference in this model was created by a conscious consumer using the manual system. In addition, the fact that the model period was limited and was carried out at a time when the light could be used efficiently increased the margin of error in the simulation result and the working model result. The user in the manual system turned off the light every time he left the room and tried to prevent energy waste when the light intensity was slightly higher than it should be. Despite all these efforts, the user of the manual system could not catch the energy efficiency in automation. In this measured data, power consumption in the automation scenario was determined using the Legrand brand smart fuse on the panel. In the classical scenario, the system's on time was

recorded and a theoretical calculation method was used.

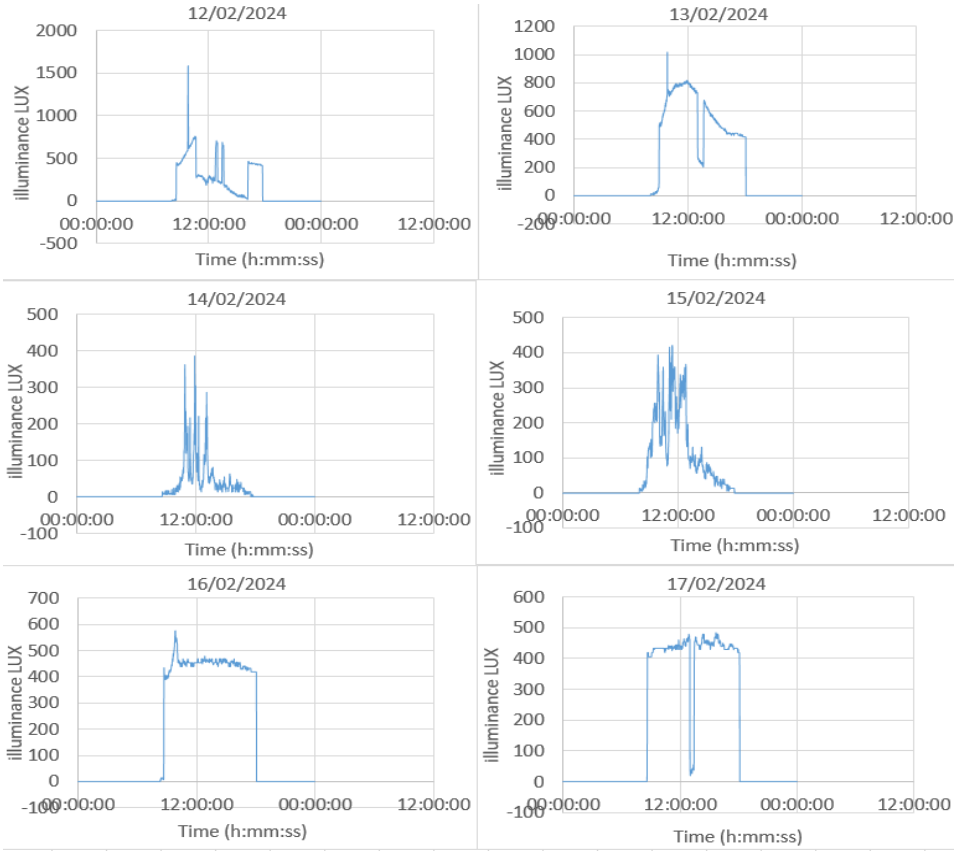

Figure. 6. 6-day light intensity data.

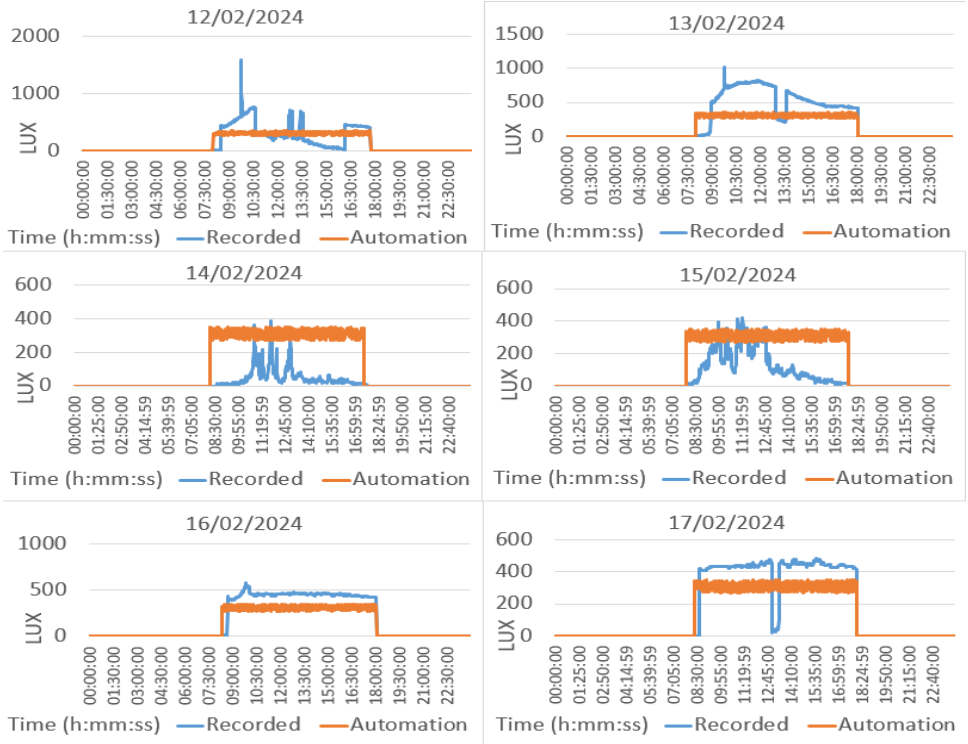

Figure. 7. Light intensity values obtained when the automation is running.

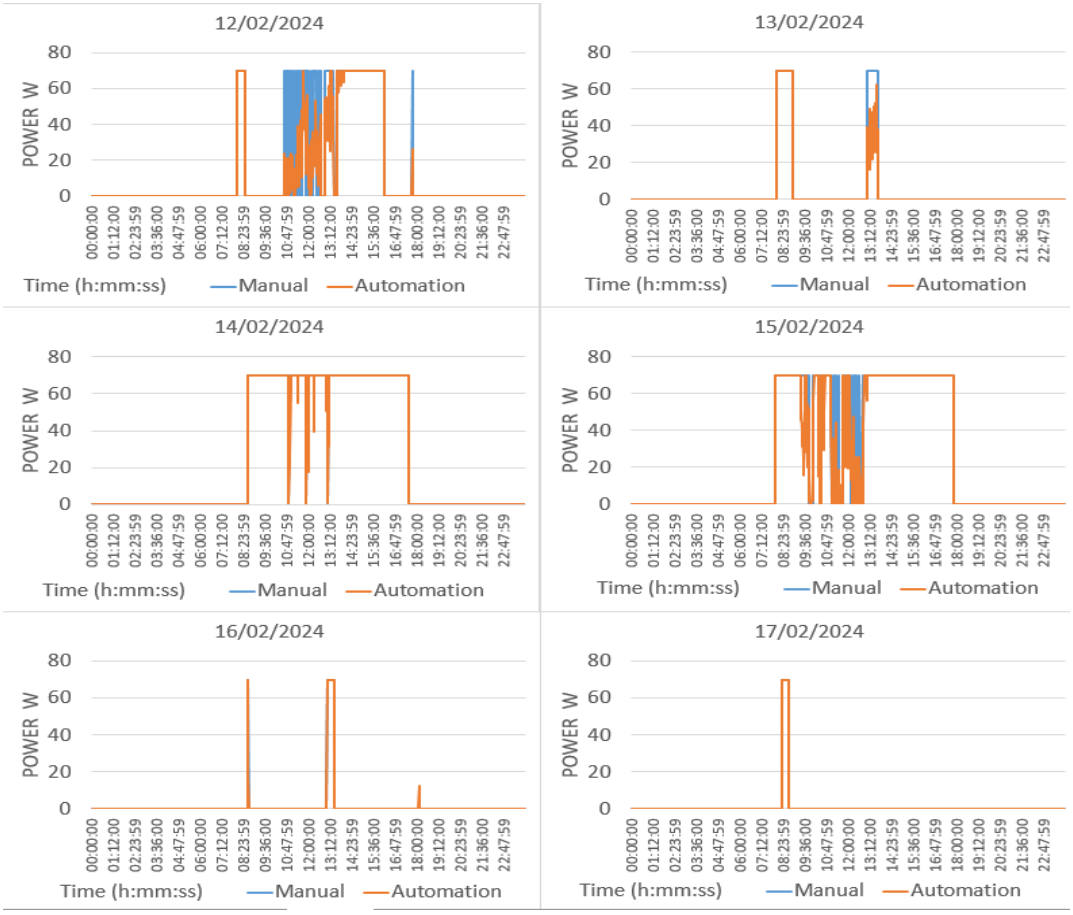

Figure. 8. Energy consumption.

III. DISCUSSION

Based on the data obtained from the research, as shown in Figure 6, it was observed that the light level in the room was particularly high during the morning hours. On some days, the lighting level exceeded 1000 lux, creating an uncomfortable working environment. The average lighting level during working hours was approximately 450 lux. While such fluctuations may not be critical in environments without automation systems, improper lighting levels can cause issues such as eye strain, headaches, and distraction, while low lighting reduces productivity, and excessive lighting causes eye strain and discomfort in the workplace. Over time, this negatively affects employees' motivation and performance and requires regulation. When the automation system was activated, as shown in Figure 7, the set lux level was consistently maintained, increasing employee comfort throughout the workday and maximizing work efficiency. However, detailed analyses revealed that the high adjustment frequency of the automation system caused oscillations in the lighting levels.

These oscillations could be minimized by reducing the sampling frequency.Energy consumption analysis shows that, over six days, when the system's status (on or off) was considered, the average hourly energy consumption for the manually controlled system was calculated to be 10.98 W. On the other hand, the automation system consumed 10.09 W of energy over the same period, showing that the automation system consumed 0.9 W less energy than the manual system. In real-time tests, the automation system was found to be 8% more efficient than the manual system. The energy saving with 8 lamps of 8W each resulted in a total savings of 130W over 6 days, considering only the lighting. In the manual system, users tried to save energy by turning off the lights when leaving the room and intervening when light levels were high. However, these efforts could not prevent the manual system from reaching the high energy efficiency of the automation system. The limited test duration and the fact that the study was

conducted during a period with abundant natural light increased the error margin between simulation and actual test results. Nevertheless, energy efficiency is critical for sustainability today. Automation systems optimize energy consumption, providing both economic savings and minimizing environmental impacts.In the manual system, the user attempted to prevent energy waste by turning off the lights when leaving the room and intervening when the light levels were high. However, these efforts could not bring the manual system to the same energy efficiency level as the automation system. In conclusion, this study demonstrates the superiority of automation systems in terms of energy efficiency and emphasizes the importance of their widespread adoption. Most automation systems used today generally focus on a single dimension. For example, in lighting automation, remote control or dimming operations are prioritized, while smart home systems offer remote control and scenario-based control options in the context of curtain control.

However, in active building automation systems, particularly in offices or public buildings, the integrated operation of lighting, curtain, and shutter systems is less common.The use of automation systems not only provides energy savings in various scenarios but also optimizes lighting levels in industrial environments, thereby enhancing worker safety and productivity. Moreover, by integrating machines and equipment, preventive maintenance can be carried out, reducing operating costs and ensuring uninterrupted production. In public institutions, these systems increase energy efficiency, reduce fossil fuel consumption, and lower carbon dioxide emissions. This way, energy savings also reduce environmental impacts and enable institutions to adopt a more environmentally friendly approach.Automation systems not only save energy but also optimize energy consumption over time and reduce maintenance needs. This leads to a significant decrease in overall operating costs. Moreover, reducing environmental impacts and achieving sustainability goals provides broader societal and economic benefits in the long run. Considering the initial investments, the cost-effectiveness of automation systems becomes clear when factors such as sustainability and energy efficiency are taken into account. An increase in employee comfort is also an important factor; well-managed aspects such as lighting, temperature, and air quality improve employee satisfaction and productivity. These improvements translate into fewer mistakes, higher productivity, and lower absenteeism rates, leading to further savings in operating costs.

IV. CONCLUSION

These Visual comfort is a critical factor for employee performance and overall satisfaction. Automation systems not only save energy but also optimize visual comfort. Lighting and curtain automation maintains the lighting balance of the space by enabling more efficient use of natural light. This ensures that the intensity of indoor illumination is kept at the desired levels and thus increases the comfort of employees. This dual benefit of automation systems shows how important it is to consider energy efficiency and visual comfort together. In the future, the wider use of such intelligent systems will provide significant gains in terms of both energy savings and visual comfort.

This study aims to maintain the ambient light level at an optimum level and ensure minimum energy consumption through the simultaneous use of different automation elements this study reveals that the average illumination level during working hours was approximately 450 lux, with some days exceeding 1000 lux, leading to discomfort in the workspace. Following the implementation of the automation system, the predefined lux level was consistently maintained, enhancing employee comfort and maximizing work efficiency. Working model show indicating a reduction of about 0.9 W. Real-time tests showed that the automation system was approximately 8% more efficient than the manual system. For a total of 6 days, the system saved 130W in lighting alone in a 20m2 room, this saving means that as a result of six days of automation, almost no costs are incurred on the seventh day compared to conventional use. Which corresponds to an annual value of 7200W per 20m2. Considering an entire 200m2 office, this system provides an annual saving of 72kW in an office.

Overall, the findings highlight the effectiveness of automation systems in reducing energy consumption and improving workplace comfort, underscoring their potential benefits. This study is expected to help increase the prevalence of such automation systems and optimize energy savings.

STATEMENT OF CONTRIBUTION RATE
Authors' contribution rates to the study are equal.

CONFLICTS OF INTEREST
They reported that there was no conflict of interest between the authors and their respective institutions.

RESEARCH AND PUBLICATION ETHICS
In the studies carried out within the scope of this article, the rules of research and publication ethics were followed.

REFERENCES

[1] Global ABC, "2013 Global Status Report For Buildings And Construction",2018.12.01, pp.1-48, Accessed (14.3.2024), Available: https://globalabc.org/sites/default/files/2020-09/2017%20GlobalABC%20GSR%20.pdf.
[2] Dilaura D. , Houser K. , Mistrick R. ,Steffy G. "The IES Lighting Handbook, 10th Edition", 2011,Zumtobel, ISBN 978-3-902940-22-3.
[3] European Commision, Energy Performance of Buildings Directive, 2010 Accessed:(14.3.2024). Available: https://energy.ec.europa.eu/topics/energy-efficiency/energy-efficient-buildings/energy-performance-buildings-directive_en
[4] Zissis G., Karlicek, R., Sun, CC., Zissis, G., Ma, R. "Energy Consumption and Environmental and Economic Impact of Lighting: The Current Situation." Handbook of Advanced Lighting Technology. Springer, Cham., 2016. https://doi.org/10.1007/978-3-319-00295-8_40-1
[5] Green Buildings and Energy Star [Online]. Accessed (14.3.2024). Available: https://www.energystar.gov/buildings/about-us/green-buildings-and-energy-star
[6] U.S. Energy İnformation Administration, issues in International Energy Consumption Analysis: Electricity Usage in India's Housing Sector", 2014, Accessed (14.3.2024), Available: https://www.eia.gov/analysis/studies/international/consumption/pdf/issues_itl_energyconsumptionanalysis.pdf.
[7] Candra o., Ulfah h. Et all," Daylight And Artificial Lighting Integration In Achieving Lighting Uniformity In Educational Building",2023, https://doi.org/10.20885/jars.vol7.iss1.art5
[8] Dehghani-Sanij, A. "Providing Thermal Comfort for Buildings Inhabitants Through Natural Cooling and Ventilation Systems: Wind Towers. In: Sayigh, A. (eds) Achieving Building Comfort by Natural Means. Innovative Renewable Energy". Springer, Cham. 2022, https://doi.org/10.1007/978-3-031-04714-5_17
[9] Kakoulli, Christina, Alexis K., and Michalis P. M. "A Review of Field Measurement Studies on Thermal Comfort, Indoor Air Quality and Virus Risk" Atmosphere 13, no. 2: 191. https://doi.org/10.3390/atmos13020191
[10] Grand View Research, "Smart Home Automation Market Size, Share & Trends Analysis Report By Component (Hardware, Software, Service), By Technology, By Application, By Fitment, By Region, And Segment Forecasts, 2023 - 2030",2022
[11] Daurat A, Aguirre A, Foret J, Gonnet P, Keromes A, Benoit O. "Bright light affects alertness and performance rhythms during a 24-h constant routine. Physiol Behav. 1993 May;53(5):929-36. doi: 10.1016/0031-9384(93)90271-g.
[12] Zumtobel,"The Lighting Handbook" ,6th edition, April 2018, ISBN 978-3-902940-72-8
[13] Belcher, M.C. and Kluczny, R.M., , "The effects of light on decision making: Some experimental results.Proceedings of the CIE 21st Session", volume I. Venice and Vienna: International Commission onIllumination, pp. 354–357" 1987.
[14] Rasouli Kahaki, Z., Jahangiri, H., Smith, A. P., & Kazemi, R. Subjective and objective survey of office lighting: effects on alertness, comfort, satisfaction, and safety. La Medicina del lavoro, (2022) 113(3), e2022024. https://doi.org/10.23749/mdl.v113i3.12371
[15] Hunt, D. R. G. "The use of artificial lighting in relation to daylight levels and occupancy." Building and environment 14, no. 1 (1979):21- 33.
[16] Yaser J., Gökhan, K.. "Examining the Efficiency of Automation in Container Terminals". Journal of transportation and logistics, 7(1):137-155. ,2022, doi: 10.26650/jtl.2022.1039692
[17] Sven, Scholz, . "Improving the Efficiency of Automated Transit Systems Compared to Traditional Train Operation". 15th International Conference on Automated People Movers and Automated Transit Systems 2016 197-205. doi: 10.1061/9780784479797.019
[18] Tulub, Valentyn "Methods of increasing the level efficiency of automated systems". Sistemi ta tehnologiï,. 2023. doi: 10.34185/1562-9945-4-147-2023-08
[19] Neelam, V., Anjali, J. "Optimized Automatic Lighting Control in a Hotel Building for Energy Efficiency",2018, 168-172. doi: 10.1109/PEEIC.2018.8665417
[20] Sinoplu, M., & Ceyhan, E. B. (2023). Artificial intelligence-assisted energy management in smart buildings: A review. UMÜFED International Journal of Western Black Sea Engineering and Science, 5(1), 39-63.

[21] KNX Association, "KNX Overview." [Online]. Accessed (14.3.2024). Available: https://www.KNX.org/KNX-en/for-professionals/What-is-KNX/A-brief-introduction/
[22] KNX Commercial Building Management System (BMS) [Online]. Accessed (14.3.2024). Available: https://knxuk.org/2022/11/16/knx-commercial-building-management-system-bms/
[23] KNX IoT Thread for Building Automation [Online]. Accessed (14.3.2024). Available: https://www.nordicsemi.com/Products/Technologies/KNX-IoT
[24] Leizerovich, D., Quiroz, I. "High-power DALI." Patent (2021).
[25] Man-Lin, W., Che-Min, K., Yi-Nan,L "DALI-2 Intelligent Lighting Control System". 2020 doi: 10.1109/IS3C50286.2020.00048
[26] Hans, G., Frank, G., Severin, D., Matthias, N. "Building automation system". 2015.
[27] Propp, Michael. Building automation system Patent ,2018.
[28] Jeffrey, J., Gloudeman., Donald, A., Gottschalk., David, E., Rasmussen., Barrett, G., Wainscott. "Software components for a building automation system based on a standard object superclass." null (1998).
[29] Christian, K., Holger, K., Falk, Z. Building automation system. 2013.